Clinical Neurophysiology Practice 4 (2019) 148–163

Contents lists available at ScienceDirect

Clinical Neurophysiology Practice

journal homepage: www.elsevier.com/locate/cnp

Review article

Neuromuscular ultrasound in clinical practice: A review

Natalia L. Gonzalez *, Lisa D. Hobson-Webb

Department of Neurology/Neuromuscular Division, Duke University Hospital, DUMC 3403, Durham, NC 27710, USA

ARTICLE INFO

Article history:
Received 19 March 2019
Received in revised form 18 April 2019
Accepted 29 April 2019
Available online 12 July 2019

Keywords:
Neuromuscular ultrasound
Carpal tunnel syndrome
Myopathy
CIDP
Ulnar neuropathy
Peripheral neuropathy

ABSTRACT

Neuromuscular ultrasound (NMUS) is becoming a standard element in the evaluation of peripheral nerve and muscle disease. When obtained simultaneously to electrodiagnostic studies, it provides dynamic, structural information that can refine a diagnosis or identify a structural etiology. NMUS can improve patient care for those with mononeuropathies, polyneuropathy, motor neuron disease and muscle disorders. In this article, we present a practical guide to the basics of NMUS and its clinical application. Basic ultrasound physics, scanning techniques and clinical applications are reviewed, along with current challenges.

Contents

* Corresponding author.
E-mail addresses: natalia.gonzalez@duke.edu (N.L. Gonzalez), lisa.hobsonwebb@duke.edu (L.D. Hobson-Webb).

https://doi.org/10.1016/j.cnp.2019.04.006
2467-981X/Published by Elsevier B.V. on behalf of International Federation of Clinical Neurophysiology.

1. Introduction

Neuromuscular ultrasound (NMUS) has developed rapidly over the last 20 years. It is now used worldwide in many academic practices and gaining wider acceptance among the general neurophysiology community. NMUS is used at the point of care, in conjunction with nerve conduction studies and needle electromyography, to augment the clinician's diagnostic capabilities. In this article, we present a practical guide to the basics of ultrasound and its current applications.

2. Basics of ultrasound, equipment and system settings

Ultrasonography is the practice of using sound waves to create an image. The transducer refers to the part of the system that comes into direct contact with the patient; it acts as both a speaker that sends sound into the tissues and as a microphone that listens for the returning sound waves. An electrical current passes through the transducer, which is converted to ultrasonic energy (*piezoelectric effect*). The transducer is therefore able to transmit sound waves to the tissue. The tissue reflects some of these waves to the transducer, where they are converted into electrical signal again. The greater the difference in *acoustic impedance* at a tissue interface (which is higher between tissues of very different densities), the more sound waves that are reflected, creating a brighter image. Image brightness is referred to as *echointensity*. Objects that appear bright, like bone, are termed *hyperechoic* and darker structures, like fluid, are *hypoechoic*.

Transducer frequency, measured in megahertz (MHz), is the most important element affecting image quality. The higher the transducer frequency, the better the image resolution. A high-frequency (12+ MHz) linear array transducer is primarily used in the evaluation of neuromuscular structures, particularly nerves. Low-frequency transducers are used preferentially in the evaluation of deeper structures, including muscle, due to greater sound beam penetration as compared to high-frequency transducers. All ultrasound imaging involves some compromise between resolution and depth of imaging. Fortunately, transducers have an adjustable range of frequencies to optimize imaging; an 18–6 MHz transducer is commonly used for neuromuscular imaging and can capture high quality images of both nerve and muscle.

Transducer array is also an important aspect of ultrasound imaging, referring to how the transducer crystals are oriented. Typically, a *linear array transducer* is used in neuromuscular ultrasound and creates a rectangular image on the screen. It provides good resolution at the edges of the images. Curvilinear transducers, which increase field of view by creating an image that is wider at the bottom than top, are preferable to evaluate deeper structures. However, resolution is lost at the lateral edges of the image with this approach. Image quality can also be affected by the width of the transducer, known as the footprint. Small footprint transducers are preferable for evaluation of areas in which limited contact with the probe surface can be made, such as in the hands and feet. All transducers have a mark or light on one side that corresponds to the left side of the ultrasound image. Standard imaging orientation is with the transducer mark towards the patient's right on axial (cross-sectional) imaging and toward the patient's head with sagittal (longitudinal) imaging.

In addition to having the appropriate ultrasound transducer, there are some basic ultrasound system settings to know when imaging – *power, gain and focal zones*. Power refers to the amount of signal that is being transmitted by the ultrasound system and is typically expressed as a percentage value. Gain is the degree of amplification for sound waves returning to the transducer. Both settings should be held constant when performing studies that aim to analyze the echointensity of nerve or muscle, as these settings affect image brightness. Focal zones refer to areas of the image where image focus is the greatest, much like with a camera. A sonographer can adjust these to optimize the appearance of region of interest within the overall image. Using no more than two focal zones is suggested.

Doppler imaging is used to document blood flow. This can be helpful in distinguishing small vessels from nerve branches and fascicles. On most systems, the color red signifies flow toward the transducer and blue indicates flow away from the transducer. Arteries are distinguished from veins not by color, but by their pulsatile flow. Power Doppler, a separate feature on many systems, is a non-directional measure of the volume of blood present in an area of interest. It is used for low flow structures, including evaluation of intraneural blood flow (Table 1).

Table 1
Essential Ultrasound Terms (Glossary of Terms | American Association of Neuromuscular & Electrodiagnostic Medicine, n.d.; Jacobson, 2017).

Acoustic impedance	The change in particle velocity in response to a change in pressure (determined by the tissue's density and the velocity at which sound travels through that tissue).
Anisotropy	The directionally dependent property of a tissue that results in an ultrasound appearance that readily changes depending on the angle of the transducer.
Doppler	A tool to measure flow, with the color red signifying flow towards the transducer and blue indicating flow away from the transducer.
Echogenicity	The ability of a tissue to reflect, rather than absorb, an echo and create brightness in an image. A hyperechoic tissue returns more signal and is therefore bright. A hypoechoic tissue absorbs the signal more than it reflects, resulting in a dark image.
Focal zones	The portion of the image where the ultrasound beam is narrow, creating a hyperechoic appearance relative to the remainder of the image. Its location can be adjusted for image optimization, like the focus on a camera lens.
Gain	The degree of amplification for sound waves returning to the transducer.
Piezoelectric effect	A property of the transducer crystal, that allows electrical signal to be converted into ultrasonic energy that is sent into the tissue. The reflected ultrasonic energy is then converted back into an electrical signal as it returns to the transducer.
Power	The rate of sound energy transferred from the transducer to the tissue.
Transducer/ Probe	The extension of the ultrasound that makes contact with the patient. It contains a crystal array that is used both to send and receive ultrasound signals.

3. Nerve ultrasound

Normal nerve appearance in the cross-sectional (axial) view is described as "honey-comb" due to the alternating, relatively hyperechoic (bright) epineurium and perineurium of fascicles (Fig. 1a). In the sagittal view, this may be seen as hyperechoic streaks parallel to the epineurium (Fig. 1b). Nerves can also be distinguished by their low *anisotropy*, meaning their appearance does not change significantly with tilting of the transducer, compared to structures with high anisotropy such as tendons and muscle (Fig. 2). Vessels can be distinguished by the presence of flow on doppler, pulsatile movement, or their collapsibility when pressure is applied.

Peripheral nerves are easily visualized in cross-section, and most can be readily traced proximally to their origin in this view, with exceptions including the sciatic nerve in the proximal thigh and the brachial plexus as it passes under the clavicle.

One of the most valuable measurements made in the evaluation of peripheral nerves is cross-sectional area (CSA). This is obtained by visualizing the nerve perpendicular to its axis and tracing the

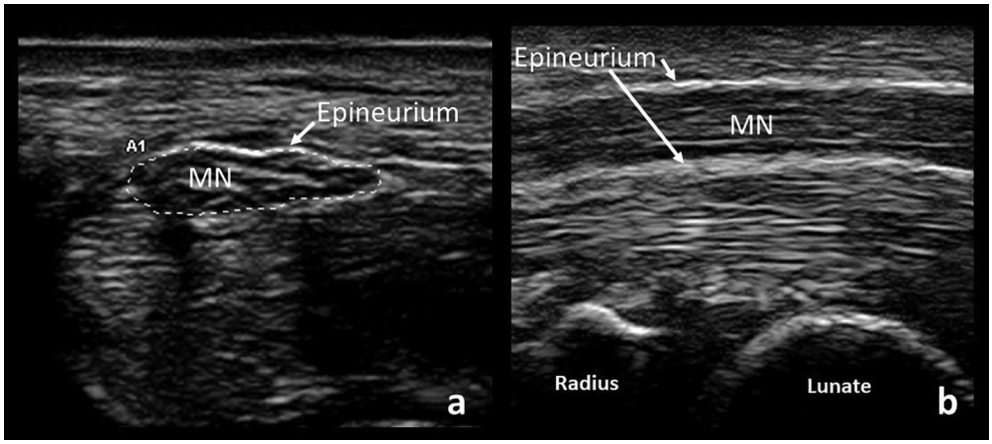

Fig. 1. Cross-sectional (a) and longitudinal (b) views of a normal median nerve (MN). Note the "honey-comb" appearance of the cross-sectional view and the surrounding hyperechoic epineurium seen in both views.

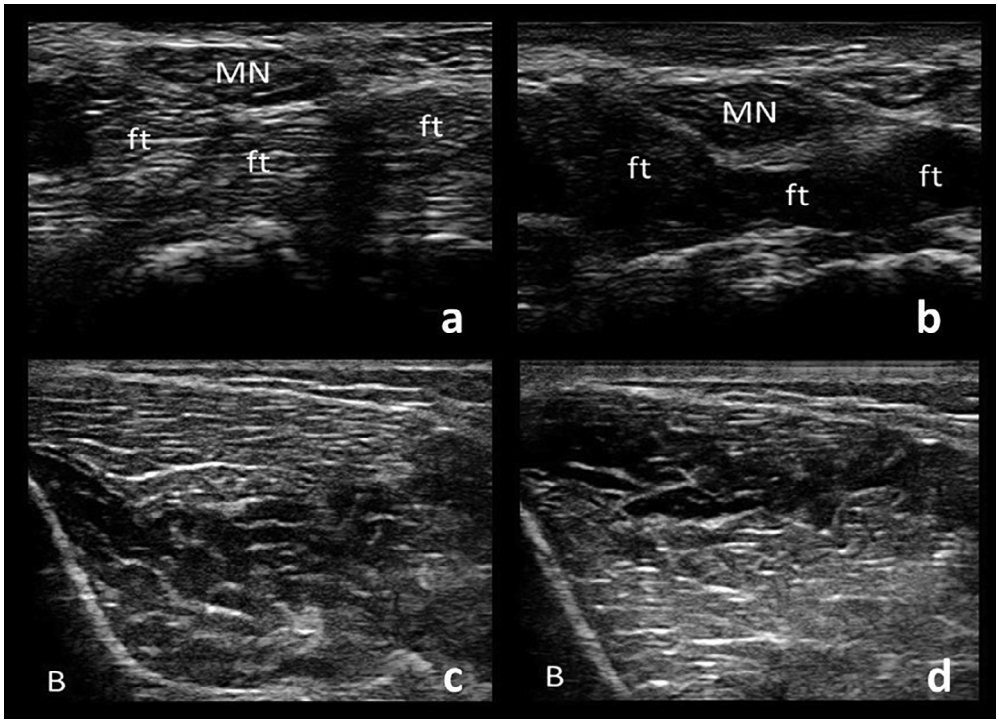

Fig. 2. Cross-sections of the median nerve (MN) and underlying flexor tendons (ft). When the transducer is angled, the median nerve remains similar in echogenicity whereas the flexor tendons demonstrate the principle of anisotropy as their appearance changes depending on the angle of the transducer (a and b). Similarly, a cross-section of tibialis anterior muscle demonstrates alternating echogenicity with tilting of the transducer in the two sections of muscle separated by an aponeurosis (c and d). Hypoechoic bone shadow is seen on the bottom left corners (B).

nerve within its hyperechoic epineurial rim (Fig. 1a). Failure to orient the transducer perpendicular to the nerve may result in inaccurate measures of CSA and poor image quality. In the upper limbs, CSA tapers off slightly as the nerve courses distally, but overall, these nerves have a relatively similar CSA from axilla to wrist. More pronounced tapering is seen in lower limb nerves. CSA is highly reliable between examiners (Mhoon et al., 2012) and correlates well with intraoperative ultrasound measurements (Bartels et al., 2008).

3.1. Focal neuropathies

The most common use of ultrasound in the EMG laboratory is to aid in localization of entrapment neuropathies. Focal nerve enlargement just proximal to the site of compression is most often present, likely a result of edema and inflammation (Cartwright et al., 2011b). However, the nerve should be evaluated a few centimeters proximal and distal to the site of compression to find the maximum point of enlargement, since (1) enlargement can happen distally and (2) due to mobility of the nerve, the location may vary with positioning. When looking at the site of compression in longitudinal views, the nerve may have a fusiform or hourglass appearance.

Other sonographic findings of entrapment neuropathies include nerve flattening, nerve hypoechogenicity (Fig. 3b), loss of nerve mobility, and increased intraneural vascularity (Fowler et al., 2014; Mallouhi et al., 2006; Nakamichi and Tachibana, 1995; Tai et al., 2012). Culprit structures resulting in compression may be

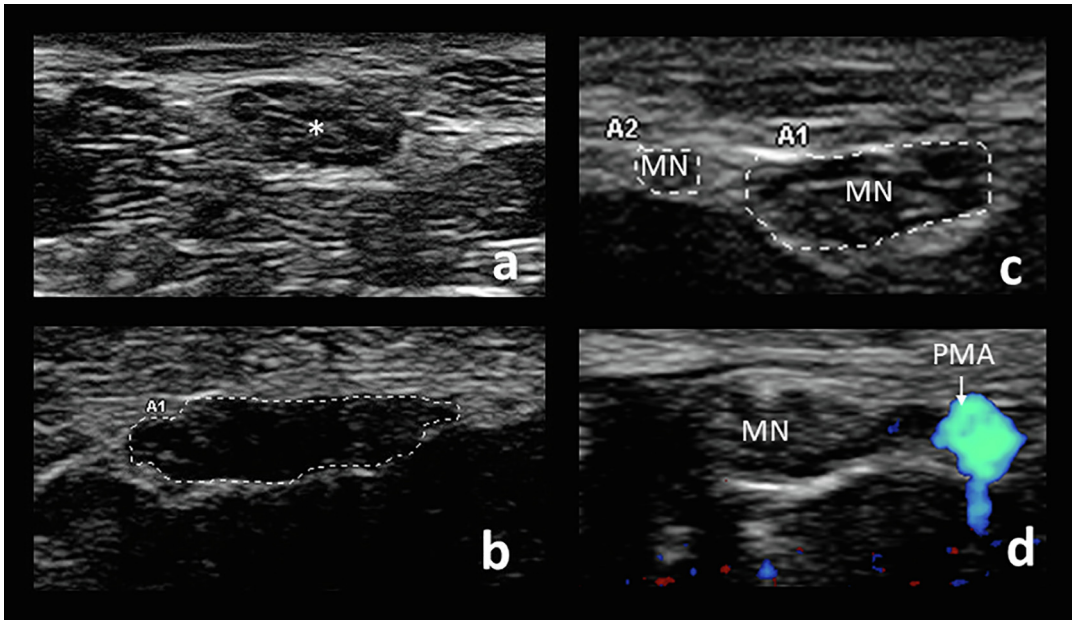

Fig. 3. Cross-sectional views of a normal median nerve (asterisk) at the wrist (a) compared to a hypoechoic, flattened, enlarged median nerve in a patient with carpal tunnel syndrome, with a CSA measuring 17 mm^2 (b). Common anatomical variants include bifid median nerve (MN) (c) and a persistent median artery (PMA), seen by doppler (d).

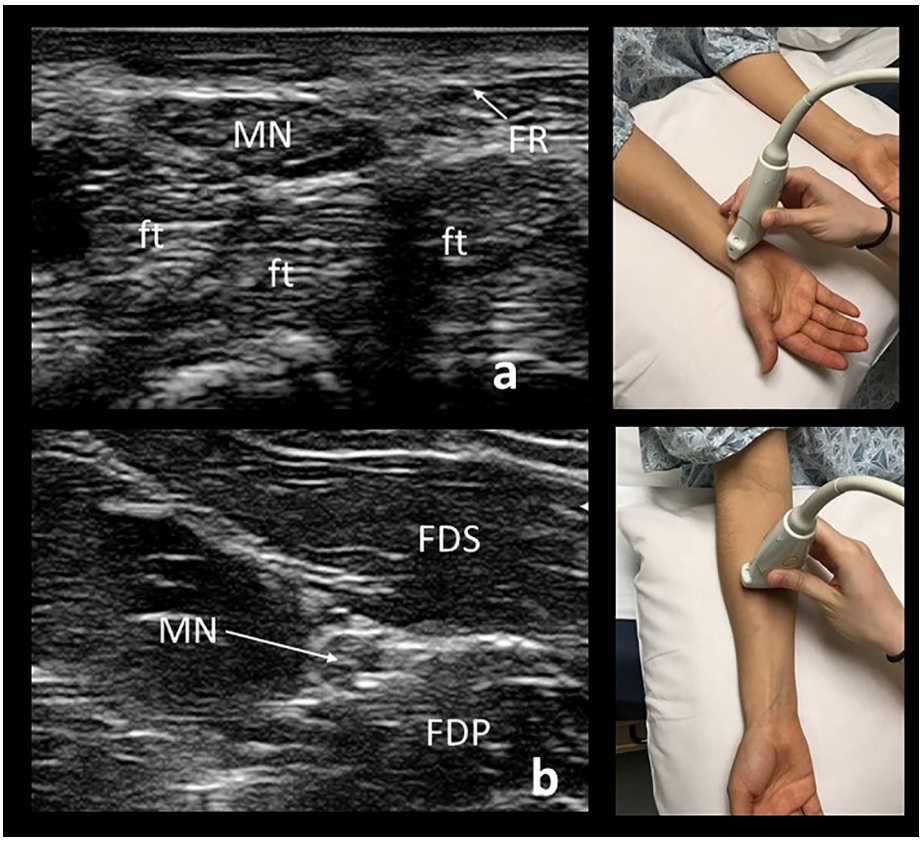

Fig. 4. A cross-sectional view of a normal median nerve (MN) when imaged at the distal wrist crease, lying above the flexor digitorum tendons (ft) in the carpal tunnel (a). For evaluation of carpal tunnel, the CSA at the wrist should be compared to the CSA in the mid-forearm (b).

identified. Finally, although not as frequently done, imaging of distal, denervated muscles may demonstrate atrophy and hyperechogenicity (Hobson-Webb et al., 2008). Assessment of these findings is important in understanding the etiology of any focal nerve entrapment as outlined in the following sections.

3.1.1. Median neuropathy at the wrist (carpal tunnel syndrome)

When imaging the median nerve, the patient may be positioned supine or sitting, with the palm facing the ceiling (Fig. 4). The median nerve is readily identified in the cross-sectional view with the transducer placed on the distal wrist crease, an external landmark

that approximates the carpal tunnel inlet. This is where the median nerve is most frequently enlarged in carpal tunnel syndrome. The nerve can then be followed proximally as it dives deep into the forearm between the flexor digitorum superficialis and flexor digitorum profundus. The nerve then passes beneath the pronator teres before coursing more superficially to join the brachial artery at the elbow. The median nerve continues alongside the brachial artery throughout the arm to the axilla. The nerve can then be seen at an 11o'clock position relative to the axillary artery.

Diagnostic cut-off values of CSA are helpful in the diagnosis of carpal tunnel syndrome (CTS), but published reference values vary depending upon the patient population used and imaging techniques. In our laboratory, a median nerve CSA of >14.6 mm^2 (two standard deviations above our control mean values) is 100% sensitive for CTS but would result in a 55% false negative rate, making such a high value of little utility in most patients (Hobson-Webb et al., 2008). Another approach to quantifying focal nerve enlargement is the median nerve wrist-to-forearm CSA ratio, which allows a patient to serve as their own internal control. This method negates differences in nerve size related to height, sex, weight and age. In an initial study, if the CSA of the median nerve at the wrist relative to its CSA in the forearm is greater than 1.4, median nerve entrapment at the carpal tunnel syndrome is likely (Hobson-Webb et al., 2008). Later studies in our laboratory demonstrated that the sensitivity of ultrasound in excluding electrodiagnostic (EDx) abnormality was 99% for CSA of less than 9 mm^2 and 97% for a wrist-forearm ratio (WFR) of less than 1.4 (Mhoon et al., 2012). Surveying multiple studies, a wrist CSA cutoff of 10 mm^2, however, is about 89% sensitive and 90% specific for clinical carpal tunnel syndrome (Fowler et al., 2014). These values hold true for patients with abnormal nerve conduction studies consistent with carpal tunnel syndrome, but changes in the nerve may be seen in patients with only clinical evidence of carpal tunnel syndrome. Based upon a restrospective study of over 1000 consecutive patients with CTS who presented to our laboratory, we utilize a conservative cutoff of a median wrist CSA of 14 mm^2 or a wrist-to-forearm ratio of 1.8 to diagnose median neuropathy at the wrist in patients with clinical symptoms of carpal tunnel syndrome and normal EDx studies (Billakota and Hobson-Webb, 2017).

Aside from nerve enlargement, there are other ultrasound findings seen at the wrist that may suggest focal compression of the median nerve. These findings are all subjectively rated and somewhat difficult to quantify, and consequently only should be used to support a diagnosis of CTS. The nerve can become hypoechoic (seen best in cross-section) (Cartwright et al., 2011b; Tai et al., 2012). Increased intraneural blood flow can also be seen and is defined as the presence of blood flow on sagittal doppler imaging of the median nerve at the wrist (Mallouhi et al., 2006). The median nerve can also lose mobility. In patients without median nerve entrapment, wrist flexion results in the median nerve diving deep into the underlying flexor tendons of the carpal tunnel. In those affected by CTS, the nerve remains between the flexor retinaculum and flexor tendons (Nakamichi and Tachibana, 1995).

Anatomical variants may be seen on ultrasound imaging. When the median nerve begins to divide before its entry into the carpal tunnel, it is termed a bifid median nerve (Fig. 3c). The frequency of bifid median nerves is approximately 10–15% across populations and is not indicative of disease, although patients with bifid median nerves may be at increased risk developing CTS (Bayrak et al., 2008). If there appear to be multiple median nerve branches, doppler should be used to confirm that the branch is not a vessel, as the persistent median artery is often associated with the bifid nerve. The CSAs of each nerve branch are then measured and added to obtain the total area. The cutoff for the diagnosis of carpal tunnel syndrome in the case of a bifid median nerve has been suggested to be a total cross-sectional area greater than or equal to 11 mm^2 (Bayrak et al., 2008). Identifying the presence and location of a persistent median artery (Fig. 3d) can be helpful to a surgeon if carpal tunnel release is pursued (Padua et al., 2012).

Etiologies other than typical CTS can cause median neuropathy at the wrist and present with similar clinical and EDx findings. This is a leading reason that advocates of NMUS recommend concurrent imaging studies in all patients with mononeuropathies. Alternative causes for focal median neuropathy at the wrist can be identified by ultrasound and include traumatic neuromas, schwannomas, lipofibromatous hamartomas, ganglion cysts, thrombosed persistent median arteries, tenosynovitis of the flexor tendons, accessory muscles, abscesses, and compressive gouty tophi (Elsaidi and Wiesler, 2004; Hobson-Webb and Walker, 2004; Kele et al., 2002; Padua et al., 2012). This structural information cannot be provided by EDx testing alone. In one study, ultrasound used in the evaluation of mononeuropathies modified the diagnostic and therapeutic path in 42% (Padua et al., 2012).

Although nerve ultrasound carries many advantages, preoperative CSA cannot be used to predict outcomes from surgical decompression of the carpal tunnel (Bland and Rudolfer, 2014). As with EDx studies, the role of ultrasound after carpal tunnel release remains unclear. Over months to one year after surgical decompression, the median nerve CSA at the wrist decreases as compared to patients undergoing conservative management (Smidt and Visser, 2008; Vögelin et al., 2010). However, there is not a clear correlation between poor postoperative outcomes and CSA at the wrist, and some nerve enlargement may remain in asymptomatic patients after successful carpal tunnel release (Smidt and Visser, 2008; Vögelin et al., 2010). As a result, the main application of post-operative NMUS may be to assess for development of compressive scar tissue or previously unidentified causes of the symptoms. This is another argument in favor of routine imaging at the time of initial diagnostic testing.

3.1.2. Ulnar neuropathy at the elbow

The ulnar nerve is evaluated with the patient supine and with the arm flexed to approximately 90 degrees at the elbow with the back of the hand rested on the pillow (Fig. 5e). A towel placed under the elbow can make this more comfortable for the patient. The ulnar nerve can then be visualized continuously from the wrist to the axilla. It lies superficial at the wrist within Guyon's canal, adjacent and medial to the ulnar artery (Fig. 5a). In most patients, the ulnar nerve follows along with the artery, medially and superior to the flexor digitorum profundus (Fig. 5b), to the upper third of the forearm. There, the ulnar nerve separates from the artery and courses superficially to enter the cubital tunnel between the two heads of the flexor carpi ulnaris (Fig. 5c). The nerve then passes into the epicondylar (ulnar) groove at the elbow, defined by the olecranon and medial epicondyle (Fig. 5d). Proximal to the elbow, the nerve runs anterior to the medial triceps brachii and ends at the 2o'clock position relative to the axillary artery in the upper arm.

About 75–80% of lesions at the elbow are localized to the epicondylar groove and about 20–25% to the cubital tunnel (Omejec and Podnar, 2015, 2016). The upper limit of normal ulnar nerve CSA is 8–11 mm^2 at the elbow with 10 mm^2 used as the most common diagnostic cut-off value (Beekman et al., 2011). Imaging the nerve proximal to the elbow provides a proximal CSA comparison, but it can also rarely be the location of ulnar nerve compression at the arcade of Struthers (Sivak et al., 2016). The wrist is another potential site of compression (Vanderpool et al., 1968) and should be evaluated when performing ulnar nerve ultrasound for possible entrapment neuropathy.

Precise localization at the elbow is important as the etiologies of ulnar neuropathy at the cubital tunnel vs at the epicondylar groove are different and management should therefore be considered dif-

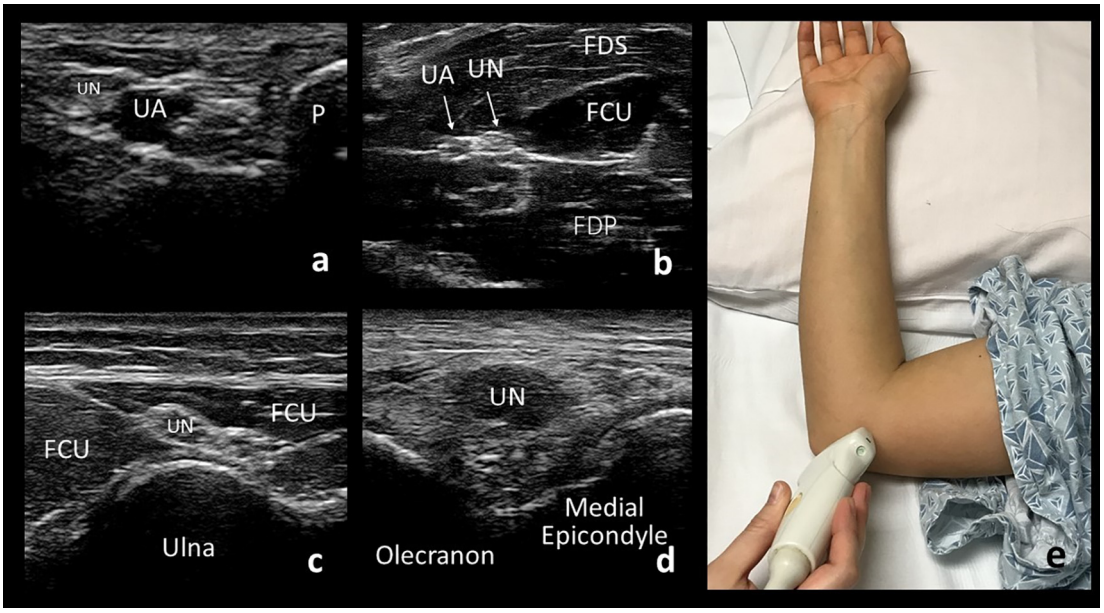

Fig. 5. Cross-sectional views of the ulnar nerve (UN) at the wrist (a), forearm (b), cubital tunnel (d), and epicondylar groove (d). UA: ulnar artery, P: pisiform bone, FDS: flexor digitorum superficialis muscle, FCU: flexor carpi ulnaris muscle, FDP: flexor digitorum profundus muscle. Demonstration of patient positioning for evaluation of the ulnar nerve at the elbow (e).

ferently (Omejec and Podnar, 2016; Simon, 2018). Specifically, ulnar neuropathy at the cubital tunnel is typically caused by entrapment and may benefit from surgical decompression, whereas ulnar neuropathy at the epicondylar groove is often caused by external compression or stretching due to positioning and may not benefit from surgical intervention (Omejec and Podnar, 2016; Simon, 2018). Although precise localization can be done with short-segment NCS, ultrasound has the added benefit of being able to visualize the source of compression and to identify cases of compression at two sites (Omejec and Podnar, 2015).

A recent retrospective review of 64 patients with electrodiagnostically confirmed ulnar neuropathy found that 25% were non-localizing. In these 16 patients, the addition of ultrasound aided localization of 13 (Pelosi et al., 2018). These findings are similar to those presented in another 2018 publication of 56 patients with ulnar neuropathy. In the 12 patients with non-localizing studies, ultrasound was successful in identifying the site of pathology in all (Alrajeh and Preston, 2018). As with median neuropathy at the wrist, ultrasound can aid in not only finding the site of pathology but also in identifying its cause. These may include intraneural or extraneural ganglion cysts, anomalous anconeus epitrochlearis muscle, lymphatic malformations, schwannomas, abscess and osteophytes (Chang et al., 2017; Dekelver et al., 2012; Filippou et al., 2010; González Pérez et al., 2017; Liu et al., 2016; Lugão et al., 2017).

Intraneural vascularity of the ulnar nerve can be evaluated by doppler, placing the transducer longitudinally over the point of maximal nerve enlargement. Increased intraneural vascularity is associated with more severe disease and ultimately, axonal loss (Frijlink et al., 2013). Hypoechogenicity may be seen, but this can be difficult to interpret since at the level of the medial epicondyle, the nerve usually is more hypoechoic than elsewhere (Stewart, 1987).

The presence of subluxation (dislocation of the ulnar nerve over the medial epicondyle during elbow flexion) or snapping triceps (dislocation of the triceps brachii over the medial epicondyle during elbow flexion) can be identified by ultrasound, although the clinical significance of their presence is unclear (Beekman et al., 2011). Approximately 20% of asymptomatic individuals may have ulnar nerve subluxation and there is limited evidence that it may actually protect against development of ulnar neuropathy at the elbow (Leis et al., 2017).

3.1.3. Radial neuropathy

The radial nerve is best evaluated with the patient supine and with the elbow slightly flexed and pointed towards the examiner, so that the posterior arm is accessible (Fig. 6). A towel can be placed under the elbow to elevate the humerus. At the axilla, the common radial nerve lies at the 5o'clock position relative to the axillary artery. The radial nerve can be identified as it runs along the humerus in the mid-arm and followed distally to the posterolateral elbow (Fig. 6a).

The common radial nerve bifurcates into deep and superficial branches (Fig. 6b). The superficial branch follows the radial artery deep to the brachioradialis along the radius, and at approximately the point of the distal one-third of the forearm, it pierces the extensor fascia and travels subcutaneously over the anatomical snuffbox to supply sensation to an area that includes the posterior first to third digits and the lateral dorsal hand. The deep branch of the radial nerve supplies the supinator and extensor carpi radialis brevis muscles. It becomes the posterior interosseous nerve after passing through the arcade of Frohse between the two heads of the supinator. It then supplies the extensor muscles of the forearm.

Radial nerve ultrasound has been used to identify areas of focal compression, including identifying unexpected "double crush" lesions affecting both the common radial nerve and the deep branch, nerve discontinuity and trauma. Normal radial nerve cross-sectional area is typically less than 10 mm^2 in the upper arm and antecubital fossa; the superficial radial nerve is 1–3 mm^2 in size, and the normal posterior interosseous nerve cross-sectional area measures approximately 2 mm^2 (Cartwright et al., 2008). Ultrasound has been shown to augment electrodiagnosis of radial neuropathy either by confirmation of electrodiagnostic studies or by providing additional information in 84% of patients (Dietz et al., 2016).

3.1.4. Fibular neuropathy at the fibular head

The fibular nerve can most easily be examined in continuity in the lateral decubitus position. It is readily identified at the fibular

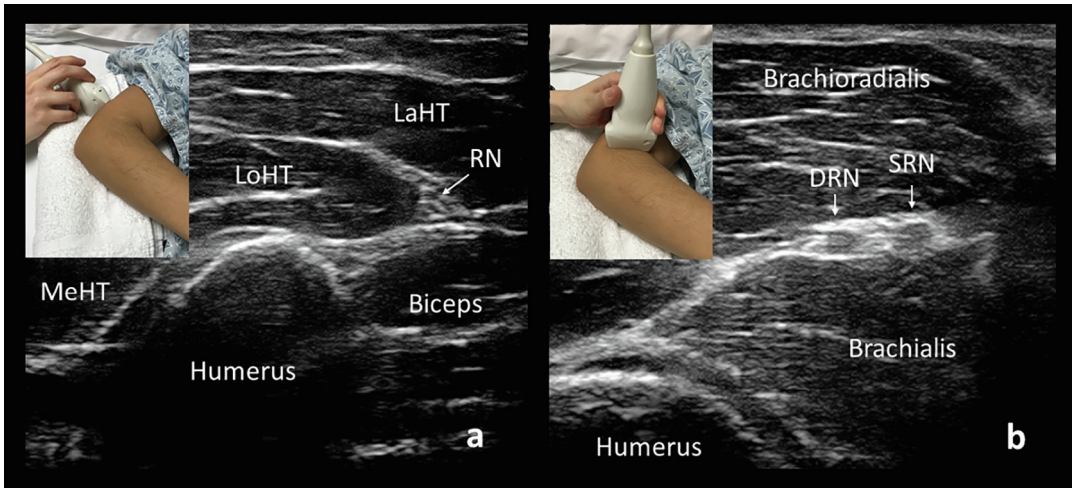

Fig. 6. Cross-sectional views of the radial nerve (RN) above the elbow (a) and at the bifurcation into the deep branch of the radial nerve (D) and superficial branch of the radial nerve (S). MeHT: medial head of the triceps brachii, LoHT: long head of the triceps brachii, LaHT: lateral head of the triceps brachii.

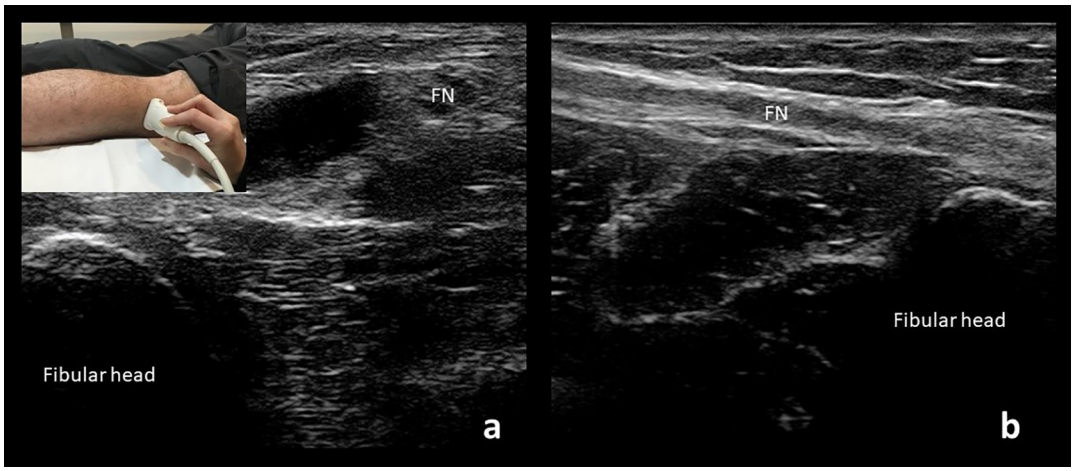

Fig. 7. Cross-sectional (a) and longitudinal (b) views of the fibular nerve (PN) just above the fibular head. Probe placement for the cross-sectional view at the fibular head is demonstrated on the top left corner.

head (Fig. 7), where it can be traced proximally to the distal sciatic nerve within the upper popliteal fossa and distally to where it splits into the superficial and deep fibular nerves. After this point, the branches are difficult to visualize as they dive deeply. Careful examination of the nerve can also reveal a branch contributing to formation of the sural nerve in some individuals. The nerve is usually smaller than 12 mm^2 at the level of the fibular head where it is most frequently compressed, (Cartwright et al., 2008; Poage et al., 2016) but care must be taken to image a true cross-section of the nerve. Given the nerve's course around the fibula, it is easy to mistakenly obtain an oblique view of the nerve and overestimate its size. Recent studies have shown that a hypoechoic fibular nerve may be seen in neuropathy, even when the overall size of the nerve is normal (Lee et al., 2016).

Fibular neuropathy at the fibular head is the most common mononeuropathy in the lower extremity (Hobson-Webb and Juel, 2017). Common causes include weight loss, prolonged immobility, and frequent crossing of the legs (Hobson-Webb and Juel, 2017).

NMUS is used for identification of potential structural causes of common fibular neuropathy including intraneural ganglion cysts, lipomas, and abnormal biceps femoris anatomy (Cartwright et al., 2008; Grant et al., 2015; Heckmatt et al., 1982; Visser, 2006). In one study, NMUS identified intraneural ganglia in 18% of cases of fibular neuropathy at the fibular head that had presented with foot drop (Visser, 2006). Particularly in patients without risk factors for fibular neuropathy, NMUS is essential in identifying structural causes that require surgical intervention.

3.1.5. Tibial neuropathy and tarsal tunnel syndrome

The sciatic nerve divides into the tibial nerve and common fibular nerve in the distal thigh. The tibial nerve then passes through the popliteal fossa and beneath the two heads of the gastrocnemius. It re-emerges just proximal to the medial ankle, then passes under the flexor retinaculum, which forms the roof of the tarsal tunnel. Other structures within the tarsal tunnel include the posterior tibial artery, associated veins and the tendons of the tibialis posterior, flexor digitorum longus, and flexor hallucis longus. The tibial nerve divides into the medial and lateral plantar nerves, typically within the tarsal tunnel.

When imaging, the patient is best positioned lying prone on the examination table. The tibial nerve can be traced by ultrasound from the sciatic nerve in the posterior distal thigh and through the popliteal fossa before it dives below the two heads of the gastrocnemius. It can be difficult to visualize in the lower leg until it becomes superficial again right above the medial ankle. The nerve can then be traced through the tarsal tunnel as it divides into its medial and lateral plantar branches (Fig. 8).

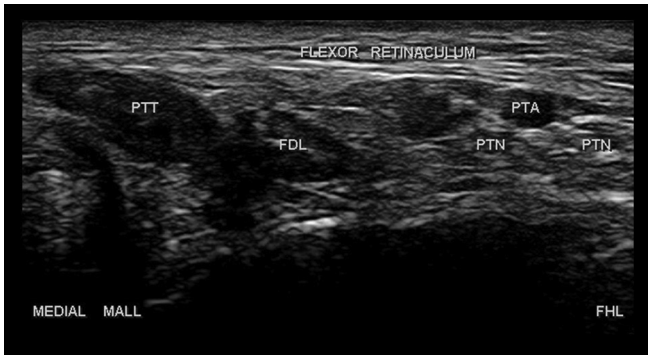

Fig. 8. Cross-sectional view of the plantar nerves (PTN) within the tarsal tunnel. PTT: posterior tibial tendon, FDL: flexor digitorum longus tendon, PTA: posterior tibial artery, Medial Mall: medial malleolus, FHL: Flexor hallucis longus.

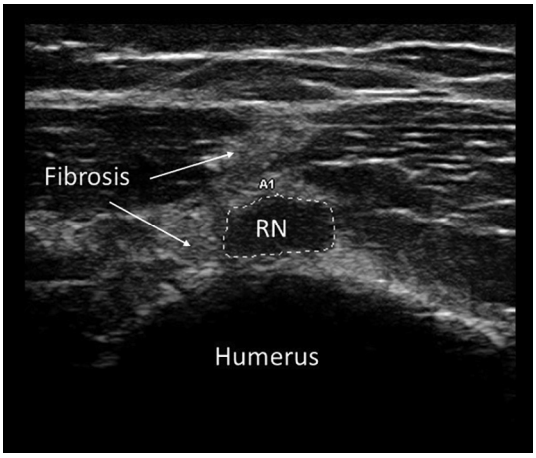

Fig. 9. Cross-sectional view of the radial nerve (RN) at the level of the mid-humerus in a patient with radial nerve palsy following a comminuted fracture of the humerus. The radial nerve here is focally enlarged (21 mm^2) and surrounded by fibrosis.

Tibial neuropathy at the ankle, or tarsal tunnel syndrome, is typically a clinical diagnosis made without definitive diagnostic criteria. Other than excluding other etiologies such as lumbosacral radiculopathy, electrodiagnostic testing is limited in its ability to diagnose tarsal tunnel syndrome. NCS may show abnormalities in the muscle action potentials of the abductor hallucis and abductor digit minimi, but the sensitivity is low. Conversely, medial and lateral plantar NCS or needle examination of the foot muscles have poor specificity (Samarawickrama et al., 2016; Tawfik et al., 2016).

NMUS may identify focal nerve enlargement of the tibial nerve and/or the medial and lateral plantar nerves at or distal to the tarsal tunnel (Samarawickrama et al., 2016). One study suggests cut-off values of 19 mm^2 for CSA within the tunnel and 1 for the within tunnel-to-proximal tunnel CSA ratio, with sensitivities of 61 and 74% respectively (Tawfik et al., 2016). We suggest obtaining a contralateral measurement for comparison where possible.

In most cases of tarsal tunnel diagnosed by EDx studies, a structural etiology was identified by ultrasound (Samarawickrama et al., 2016). Based on a study of 81 cases, the most commonly seen etiologies by ultrasound were varicose plantar veins, epineural ganglion cysts, and accessory flexor digitorum longus muscles (Fantino, 2014). Proximal to the ankle, etiologies that may compress the tibial nerve include Baker's cysts, intraneural ganglion cysts, popliteal artery aneurysms, deep venous thromboses, and by the soleal sling (Sanchez et al., 2011; Williams et al., 2012, 2009).

3.2. Traumatic neuropathies

Electrodiagnostic studies often provide inconclusive results in the first few weeks following nerve trauma. In the critical early days after a peripheral nerve injury, it may be difficult to distinguish between axontomesis and neurotmesis. This can result in delayed surgical repair and poor outcomes (Tagliafico et al., 2010). Ultrasound can change or significantly modify the pretest diagnosis or provide additional useful information in most cases of traumatic nerve injury (Padua et al., 2013). It can identify transected nerves, fibrosis (Fig. 9), pseudoaneurysm, neuroma, bony compression, callous formation, and other anatomic changes (Tagliafico et al., 2010). The addition of imaging can expedite and direct appropriate care.

3.3. Brachial plexus

Imaging the brachial plexus is more technically challenging than peripheral nerves but can provide useful diagnostic information. Be aware that the roots, trunks, and cords are hypoechoic, without the characteristic fascicular appearance of more peripheral nerves (Baute et al., 2018). The patient is examined supine with the head slightly extended and turned away from the side of interest. Begin by identifying the trachea and overlying isthmus of the thyroid in the transverse view and then move laterally to the common carotid artery, vagus nerve, and internal jugular vein (Fig. 10).

Continuing to move laterally, the C5 root will be seen arising from the anterior and posterior tubercles, that together resemble a molar tooth (Fig. 11a). The C6 root will arise with a prominent anterior tubercle that resembles a "thumbs up" sign (Fig. 11b). The C7 transverse process lacks an anterior tubercle but has a posterior tubercle that resembles the back of a chair (Fig. 11c). The C8 root does not arise from a transverse process, and the C8 and T1 roots can be difficult to visualize. In a longitudinal view, the C5 to C7 nerve roots are seen running parallel to each other as they enter the foramina of the transverse processes, a view that may identify root avulsion in the case of trauma (Fig. 11d) (Baute et al., 2018). It is important to note, however, that ultrasound is only able to visualize the ventral rami of the nerve roots distal to the vertebral bodies and so proximal lesions will not be seen.

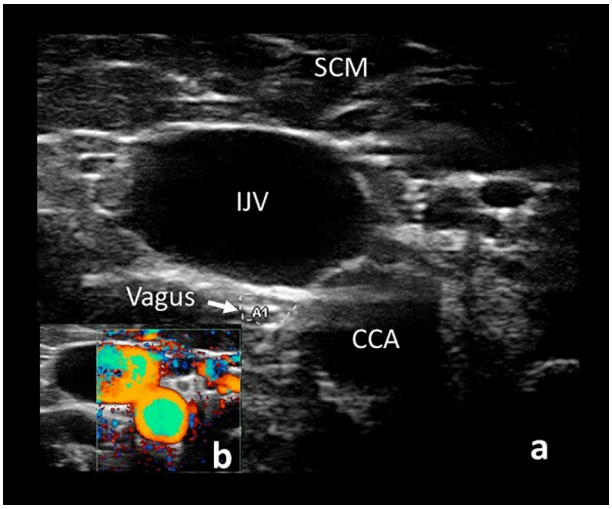

Fig. 10. View of the common carotid artery (CCA), internal jugular vein (IJV), and vagus nerve (arrow) beneath the sternocleidomastoid (SCM) (a). Confirmation of vessel location by doppler is demonstrated in the bottom left corner (b).

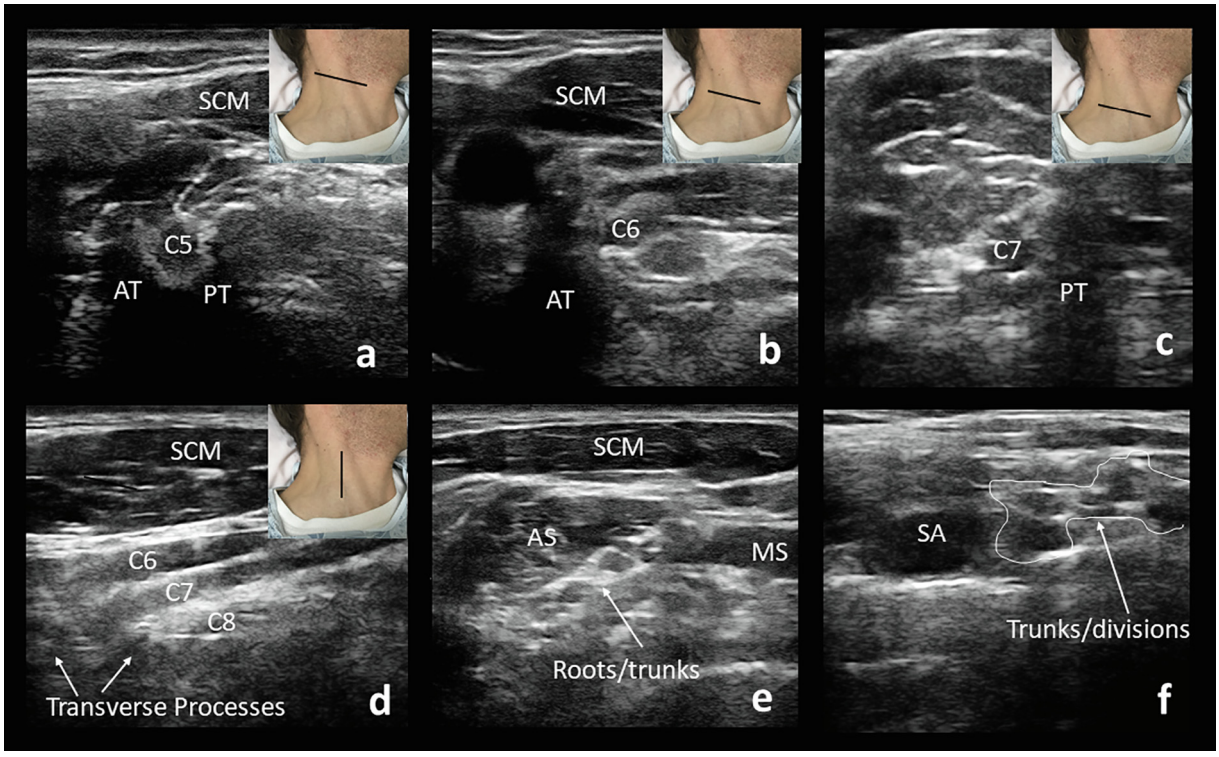

Fig. 11. The C5 nerve arises from anterior (AT) and posterior (PT) tubercles that resemble a molar tooth (a). The C6 nerve root arises from a prominent anterior tubercle, resembling a "thumbs up" sign (b). C7 transverse process lacks an anterior tubercle but has a posterior tubercle that resembles the back of a chair (c). The nerve roots can be seen exiting their foramina in a sagittal view (d). The transducer positioning is demonstrated by the black line. The roots and proximal trunks can be seen between the anterior and middle scalene muscles (e). Further laterally, the plexus appears as a "bunch of grapes" (f). SCM: sternocleidomastoid muscle, CA: carotid artery, AS: anterior scalene muscle, MS: middle scalene muscle, SA: subclavian artery.

The proximal upper (C5 and C6), middle (C7), and lower (C8 and T1) trunks arising from the roots can be seen between the anterior and middle scalene muscles (Fig. 11e). The trunks may be difficult to visualize if there is a paucity of surrounding fat, which usually provides a hyperechoic contrasting background. The subclavian artery is a useful landmark in this region. The C8 and T1 roots lie deep to the subclavian artery and the middle and upper trunk superficial to it. Further laterally, the plexus appears as a "bunch of grapes" as the trunks branch into divisions (Fig. 11f). The CSA of components of the brachial plexus can be measured and compared to the contralateral side (Baute et al., 2018).

Depending on the purpose of evaluation, other branches of the plexus can be identified. The phrenic nerve runs superficial to the anterior scalene. The dorsal scapular and long thoracic nerves pierce the middle scalene with the dorsal scapular nerve superficial to the long thoracic nerve. The suprascapular nerve comes off of the C5 root and travels laterally under the omohyoid and in a posterior direction (Baute et al., 2018).

Inferior to the clavicle, the transducer can be oriented longitudinally just medial to the coracoid process. The three cords surround the subpectoral axillary artery. The medial and lateral pectoral nerves can be seen at this level between the fascial planes of the pectoralis major and minor (Baute et al., 2018).

To visualize the terminal branches, the transducer is placed in the axilla. The radial nerve will lie posterior to the brachial artery and adjacent vein and move deep towards the humerus. The ulnar nerve lies medially and the median nerve lies laterally to the vessels. The lateral musculocutaneous nerve can be seen penetrating the coracobrachialis (Baute et al., 2018).

Ultrasound can be particularly useful for evaluation of traumatic brachial plexus lesions. For example, it is used in the evaluation of obstetrical brachial plexopathies, by the identification of neuromas or root avulsions (Smith et al., 2016). It may also identify compressive masses or compression during abduction or external rotation in the case of thoracic outlet syndrome, although the evaluation of the costoclavicular space by ultrasound is limited due to the overlying clavicle shadow (Demondion et al., 2003). Ultrasound is also increasingly being used for non-traumatic brachial plexus lesions. Brachial plexus and cervical root ultrasound are similar in sensitivity to MRI in detecting focal nerve enlargement in multifocal motor neuropathy (MMN) and chronic inflammatory demyelinating polyradiculoneuropathy (CIDP), making it a useful tool to support the clinical diagnosis when nerve conduction studies are inconclusive. In one study, sonographic enlargement of a brachial trunk was seen in 78% of patients with CIDP and in 68% of patients with MMN (Goedee et al., 2017). In a retrospective study evaluating ultrasound vs MRI in upper extremity mononeuropathies and brachial plexopathies, ultrasound was more sensitive and similar in specificity to MRI and was found to be particularly useful in identifying more multifocal nerve pathology (Zaidman et al., 2013b).

3.4. Generalized neuropathies

Aside from focal nerve entrapments and injuries, NMUS has utility in diagnosing some generalized peripheral neuropathies. Peripheral nerve enlargement is characteristic of many demyelinating neuropathies and can occur anywhere along the course of the nerve. Identification of nerve enlargement with ultrasound can support or clarify electrodiagnosis of these conditions, particularly Charcot-Marie-Tooth (CMT) disease type 1a and CIDP.

In CMT1a, there is diffuse nerve enlargement in which prominent dark fascicles are seen (Zanette et al., 2018). More subtle enlargement can be seen patients with CMT2 and other subtypes

of CMT1 (Schreiber et al., 2013; Zanette et al., 2018). Identifying widespread nerve enlargement can be a particularly useful tool in children who may not tolerate electrodiagnostic studies and in screening family members before proceeding with more expensive testing.

Acquired inflammatory polyneuropathies, including CIDP and MMN, may demonstrate multifocal nerve enlargement outside of areas of compression that sometimes correlate with conduction blocks seen on nerve conduction studies (Granata et al., 2009; Scheidl et al., 2012). The proximal upper extremities are the highest yield location to identify focal nerve enlargement in non-compressible sites in CIDP patients (Scheidl et al., 2014). This can be particularly useful in patients with multiple diseases (e.g. CIDP and diabetic polyneuropathy), in those in which inflammatory neuropathy is suspected but conduction block is not captured by NCS, and in patients in which the severity of the neuropathy may make differentiation of demyelinating or axonal neuropathy difficult based upon electrodiagnostic studies alone. Some studies have suggested a role for nerve ultrasound in assessing treatment efficacy and prognosis in CIDP (Kerasnoudis et al., 2015b; Zaidman and Pestronk, 2014).

The role of ultrasound in the diagnosis of Guillain-Barre syndrome (GBS) is still unknown, as published studies have reported varying percentages of patients with GBS possessing significantly enlarged peripheral nerves, ranging from 0% to 53% (Kerasnoudis et al., 2015a; Zaidman et al., 2013a, 2009). A significant issue with many of these studies is that nerve ultrasound often was not performed during the acute stages of the illness. Further studies are needed for a number of standardized scoring systems have been developed for nerve ultrasound, particularly for the identification and subclassification of inflammatory neuropathies (Grimm et al., 2017).

Diabetic polyneuropathy is typically a mixed demyelinating and axonal polyneuropathy and is associated with mild nerve enlargement. Most acquired axonal neuropathies demonstrate mild or no nerve enlargement (Telleman et al., 2018). A recent study, however, found peripheral nerve enlargement to be fairly widespread in the disorder (Breiner et al., 2017). Given the current data, there is not a firm role for using NMUS in the diagnosis of diabetic polyneuropathy, although newer ultrasound technologies like shear wave imaging hold promise for doing so (Dikici et al., 2017). Literature exists supporting nerve ultrasound in the evaluation of other generalized or multifocal neuropathies including leprosy and vasculitic neuropathy (Grimm et al., 2014; Martinoli et al., 2000).

Key ultrasound findings in certain neuropathies and myopathies are summarized in Table 2.

4. Muscle ultrasound

In healthy muscle, the muscle fibers are hypoechoic and the fibro-adipose and perimysial connective tissues are hyperechoic, creating a speckled pattern (Fig. 12). There is variation in muscle echogenicity depending on the patient's age and sex. In infants, muscle is more hypoechoic and has less myofascial planes, in childhood, echogenicity remains stable (Scholten et al., 2003), and in adulthood, it increases due to fatty replacement and fibrosis and does so more rapidly in advanced age (Reimers et al., 1993). Muscle in boys is slightly darker than girls, and the difference persists throughout adulthood (Zaidman and van Alfen, 2016). In addition to these challenges, muscle is highly anisotropic, and its appearance can be altered through tilting of the transducer, which alters the angle of insonation (Fig. 2). Keeping the transducer perpendicular to the muscle is essential for obtaining adequate images. Given that muscle is often located deeper than nerve, a lower frequency transducer (5–10 MHz) may be needed for some locations.

Muscle thickness is measured in the cross-sectional view of the relaxed muscle belly, from the superficial fascia to the underlying bone or deep fascia. It varies with age, sex, body habitus, and conditioning (Zaidman and van Alfen, 2016). Care must be taken not to apply too much pressure with the ultrasound transducer when measuring subcutaneous tissue and muscle thickness as compression will falsely decrease the muscle and subcutaneous tissue thickness and increase muscle echogenicity. This can be avoided with use of generous amounts of ultrasound gel. However, it should be noted that some degree of muscle compression does improve the reliability of ultrasound echointensity measures when force is standardized (Pigula-Tresansky et al., 2018).

A unique feature of ultrasound is its ability to capture dynamic images. It can be used to localize a specific muscle and confirm contraction. Situations where this may be valuable include stimulation-guided chemodenervation, technically challenging needle electromyography sites, to assess diaphragm movement, or to identify fasciculations and even fibrillations (van Alfen et al., 2011; Walker et al., 1990).

Rating muscle echointensity has proven to be a difficult task. At a basic level, the Heckmatt scale provides a method of grading this qualitative assessment of muscle echogenicity and visualization of

Table 2
Characteristic ultrasound findings of nerve and muscle disease.

Neuropathy		
Focal neuropathies	Increased CSA, hypoechoic proximal to site of entrapment, decreased nerve mobility, increased intraneural vascularity	
	Normal CSA cutoffs:	
	Median nerve at wrist	$\leq$10 mm^2 ;or WFR of 1.4 (Fowler et al., 2014; Mhoon et al., 2012)
	Ulnar nerve at elbow	$\leq$10 mm^2 (Beekman et al., 2011)
	Radial nerve at spiral groove	$\leq$10 mm^2 (Cartwright et al., 2008)
	Fibular nerve at fibular head	$\leq$12 mm^2 (Cartwright et al., 2008)
	Tibial nerve in tarsal tunnel	$\leq$19 mm^2 for CSA within the tunnel; or within tunnel-to-proximal tunnel CSA ratio 1.0 (Tawfik et al., 2016)
Hereditary neuropathies (e.g. CMT1a)	Diffuse nerve enlargement and prominent dark fascicles	
Acquired inflammatory polyneuropathies (e.g. CIDP)	Multifocal nerve enlargement outside of areas of compression	
Myopathy		
Muscular dystrophy	Hyperechoic muscle with attenuation of the underlying bone	
Inflammatory myopathy	Although likely dependent on chronicity, the most common findings are hyperechoic muscle, normal underlying bone echo, possibly increased muscle thickness, and increased vascularity.	
Motor neuron disease		
Hyperechoic muscle with decreased thickness, decreased muscle echovariation; presence of fasciculations; reduction in cervical root and peripheral nerve CSA		

CSA: Cross-sectional area; WFR: Wrist-to-forearm ratio; CMT1a: Charcot-Marie-Tooth type 1a; CIDP: Chronic inflammatory demyelinating polyneuropathy.

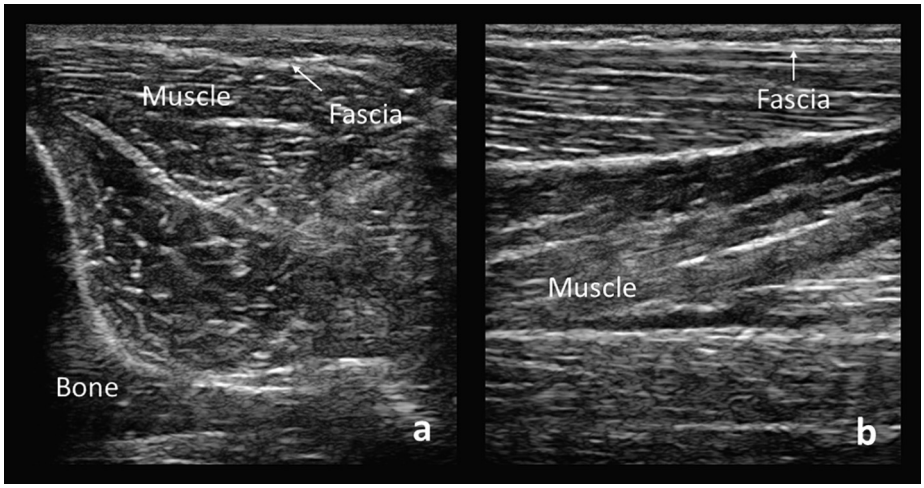

Fig. 12. Cross-sectional (a) and longitudinal (b) views of a normal tibialis anterior muscle.

the deep bony structures (Heckmatt et al., 1982). However, qualitative assessments of muscle echogenicity are strongly operator dependent (Brandsma et al., 2014; Pillen et al., 2006a,b). Quantitative methods of analysis have demonstrated strong sensitivity in neuromuscular disorders in children (Pillen et al., 2007) and have high interrater reliability (Zaidman et al., 2014). However, reference values must be specific to not only age, sex, and individual muscle but should also be specific to the ultrasound system hardware and software, restricting its use primarily to research for now. Other approaches to standardization of echointensity measures include quantitative backscatter analysis (Zaidman et al., 2008), the use of systems without post image processing (O'brien et al., 2017), and phantom-based conversions (Pillen et al., 2009).

4.1. Muscular dystrophy and congenital myopathy

The fatty replacement and fibrosis seen in muscular dystrophies results in increased heterogeneity of tissues within the muscle, which leads to hyperchogenicity on ultrasound. Additionally, there is progressive attenuation of the underlying bone signal (Heckmatt et al., 1988). Congenital myopathies similarly demonstrate hyperechogenicity, likely due to disruption in muscular architecture rather than fibrosis (Pillen et al., 2008). Atrophy may result in decreased muscle thickness and increased depth of subcutaneous tissue (Heckmatt et al., 1982). Isoechoic atrophic muscle suggests atrophy without underlying structural changes, such as in the case of disuse atrophy that has not yet undergone fatty or fibrous replacement. Less likely, this pattern can be seen in mitochondrial myopathy or acute/subacute denervation (Pillen et al., 2006a,b; Zaidman and van Alfen, 2016).

NMUS can also characterize the pattern of involvement of affected muscles, which may suggest or confirm a diagnosis. For example, in Duchenne muscular dystrophy (DMD), Becker muscular dystrophy (BMD), and limb girdle muscular dystrophies, there tends to be homogenous increase in echogenicity throughout the muscle, resulting in a fine granular, "ground-glass" appearance (Heckmatt et al., 1988). Conversely, in Bethlem myopathy, an echogenic spot is seen in the ventral and central rectus femoris where there typically is a region of central fascia (the "central shadow sign"), reflective of the initial involvement of the muscle closest to fascia (Bönnemann et al., 2003).

Preferential involvement of certain muscles can also suggest a specific diagnosis. NMUS can be used to identify clinically affected and some sub-clinically affected muscles in late-onset Pompe disease with a characteristic pattern that includes triceps and rectus femoris sparing (Vill et al., 2015; Zaidman et al., 2011). In Pompe disease, bone echogenicity is not reduced, as it is in muscular dystrophies. There is conflicting evidence as to whether NMUS is sensitive enough to be used as a screening method for newborns (Hwang et al., 2017; Vill et al., 2015). As with other diagnostic tools, care must be taken to interpret results in the context of the clinical history, physical examination, and when available, electrodiagnostic studies.

NMUS is a potential marker of disease progression and therapeutic efficacy in DMD. Echogenicity shows the most change in the proximal lower extremities in young boys (4–7 years of age) and in the upper extremities in older boys (8–15 years of age) (Jansen et al., 2012; Zaidman et al., 2017). There is likely a "ceiling effect" after the age of 12, correlating with a similar effect seen in functional measures (Jansen et al., 2012). Hyperechogenicity can also be seen in the tongue and submental muscles, which correlates with dysphagia and chewing difficulty (Van Den Engel-Hoek et al., 2012). In DMD, muscle thickness remains normal even as the disease progresses, except in muscles affected by disuse (Jansen et al., 2012).

Two types of quantitative analyses, gray scale level and quantitative backscatter analysis, have been found to be more sensitive than functional assessments for detecting muscle deterioration in children with DMD (Jansen et al., 2012; Zaidman et al., 2017). This is seen even in infants and toddlers prior to functional decline, making it a possible measure of early disease progression (Zaidman et al., 2015). Additionally, there is no apparent effect of steroids on muscle echointensity in DMD (Zaidman et al., 2017). Whether NMUS can serve as a marker of treatment response of new therapies is still unknown.

4.2. Inflammatory myopathies

In addition to supporting a diagnosis, ultrasound has potential as an indicator of disease activity in inflammatory myopathy. This is often a clinically difficult question since weakness in these patients may be due to active inflammation, but may also be due to corticosteroid use, chronic atrophy, or a comorbid condition (Sousa Neves et al., 2018). The sensitivity of muscle ultrasound in detecting histopathologically proven inflammatory myopathy has been reported as high as 82.9% (Reimers et al., 1993).

The characteristic findings in various inflammatory myopathies and the timeline of changes in acute vs chronic disease are not well established. Muscle edema on NMUS appears to be specific to acute myositis. This is seen as focal or generalized hypoechogenicity and

increased muscle thickness (Reimers et al., 1993; Sousa Neves et al., 2018). However, the more common finding appears to be hyperechogenicity with normal or increased muscle thickness, with the increased in echogenicity suspected to be due to inflammation and edema (Mittal et al., 2003; Sousa Neves et al., 2018). This finding may reverse with treatment (Mittal et al., 2003). Additionally, there may be relatively preserved visualization of the deep bony structures despite significantly increased echogenicity, in contrast to dystrophies in which the bony structures are obscured (Mittal et al., 2003). Chronic disease appears to be characterized more by fat infiltration and atrophy, with findings on ultrasound of hyperechogenicity and decreased muscle thickness (Reimers et al., 1993).

Increased muscular vascularity on power doppler appears to detect inflammatory muscle diseases of shorter duration (Meng et al., 2001). However, this is a subjective measure prone to artifact. A promising application of ultrasound is contrast-enhanced power doppler to measure local blood flow. This method utilizes microbubbles that can be destroyed by high energy ultrasound pulses. The subsequent refilling of microbubbles from outside the area of interest can then be used to calculate various vascularization measures (Weber et al., 2006). In one study, increased blood flow by power doppler had a sensitivity of 73% for histologically confirmed myositis, whereas increased T2 signal on MRI had 100% sensitivity. The specificities were similar at 88% and 91% respectively (Weber et al., 2006).

On occasion, some muscle ultrasound features may suggest a specific diagnosis. For example, increased deltoid fascial thickness is seen in patients with dermatomyositis and polymyositis (Bhansing et al., 2015). In inclusion body myositis, there is a pattern of hyperechogenicity in the flexor digitorum profundus with sparing of the adjacent flexor carpi ulnaris (Noto et al., 2014), although this pattern was also reported in a patient with myotonic dystrophy type I (Karvelas et al., 2018).

4.3. Diaphragm ultrasound

Imaging the diaphragm is easiest using an intercostal approach. Examine the patient in a supine position using a high-frequency linear array transducer oriented longitudinally in the zone of apposition, at the 9th intercostal space and just anterior to the midaxillary line. The diaphragm is measured at maximal inspiration and end-expiration (Fig. 13). The ratio of diaphragm thickness in maximal inspiration compared to expiration has a high sensitivity and specificity for neuromuscular disease in the outpatient setting (Boon et al., 2014; O'Gorman et al., 2017; O'Gorman and O'brien (2017)). The normal thickening ratio averages 1.8, with a lower limit of normal of 1.2 (Boon et al., 2013).

Diaphragm imaging can be valuable in patients with absent phrenic nerve responses on electrodiagnostic testing, particularly those where body habitus makes the study difficult. As the diaphragmatic movement is often easily visualized, ultrasound can also serve as an alternative for the radiographic "sniff test" and guide needle insertion during electromyography (Boon and O'Gorman, 2016).

5. Motor neuron disease

The role of NMUS in diagnosis and monitoring of motor neuron diseases appears promising, with a rapidly enlarging body of literature supporting its application. In motor neuron diseases, including amyotrophic lateral sclerosis (ALS) and spinal muscular atrophy (SMA), muscle ultrasound demonstrates hyperechogenicity and decreased muscle thickness, consistent with a pattern of atrophy (Arts et al., 2011). A specific muscle ultrasound measurement, echovariation, appears promising as a potential biomarker in ALS. Echovariation is a measure of echointensity range and, consequently, homogeneity(Martínez-Payá et al., 2017). ALS patients have significantly lower echovariation than controls (Martínez-Payá et al., 2017), and echovariation appears to correlate with strength and disability (Martínez-Payá et al., 2017).

Muscle ultrasound is more sensitive than EMG in detecting fasciculations, particularly in the tongue (Johansson et al., 2017; Misawa et al., 2011; O'gorman et al., 2017; Walker et al., 1990). Using certain scoring methods, fasciculations can be used for ALS diagnosis with high sensitivity and specificity with or without measures of echointensity (Arts et al., 2012; Johansson et al., 2017; Tsuji et al., 2017).

Interestingly, although not extensively studied, is the reduction in cervical root and peripheral nerve cross-sectional area on ultrasound described in patients with ALS (Cartwright et al., 2011a; Nodera et al., 2014; Ríos-Díaz et al. (2019).), likely reflective of motor axon loss. One study demonstrated small but significant reductions in ulnar nerve CSA at the wrist and forearm in all ALS variants except the primary lateral sclerosis (PLS) group, suggesting it may be useful as a marker of lower motor neuron involvement (Schreiber et al., 2015).

Ultrasound also has the potential to monitor respiratory function in ALS patients. In one study, diaphragm thickness during full inspiration (as well as the difference between thickness during

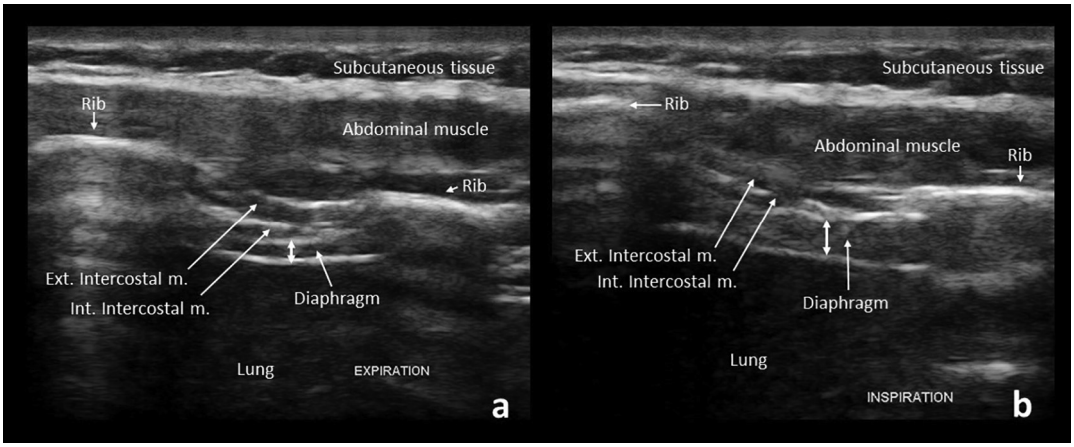

Fig. 13. Normal increase in diaphragm thickness (double-headed arrows) from expiration (a) to inspiration (b). Ext. Intercostal m.: External intercostal muscle, Int. Intercostal m.: Internal intercostal muscle.

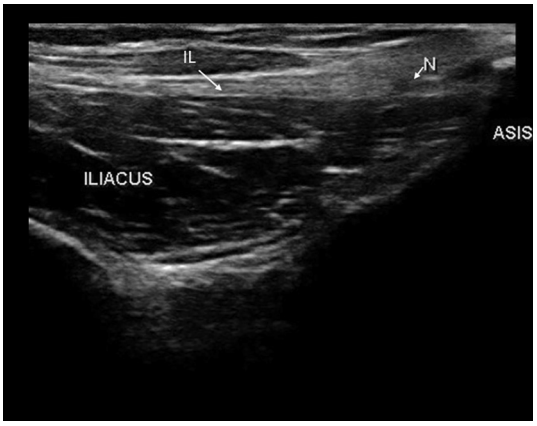

Fig. 14. The lateral cutaneous nerve of the thigh (N) passing under the inguinal ligament (IL) and above the iliacus at the level of the anterior superior iliac spine (ASIS).

inspiration vs. expiration) correlated with diaphragm compound muscle action potential (CMAP) as well as with forced vital capacity (FVC), sniff nasal inspiratory measure (SNIP), and maximal voluntary ventilation (MVV) (Pinto et al., 2016).

6. Ultrasound guidance of procedures

One of the most commonly used applications of neuromuscular ultrasound is the guidance of procedures. This includes guidance of steroid injections (such as for carpal tunnel syndrome), botulinum toxin injections (such as in the muscle for spasticity or dystonia or in salivary glands for sialorrhea), regional anesthesia, preoperative detection of nerve location, guidance of muscle and nerve biopsy, and lumbar puncture site determination (Alter et al., 2013; Jacobson, 2017; Soni et al., 2016).

Ultrasound can be particularly helpful in increasing patient safety as well as improving study quality in the EMG laboratory. It can be used to localize specific muscles to target EMG needle placement, which is particularly helpful in muscles such as the diaphragm that carry a risk of pneumothorax. It can also be used to localize nerves and therefore guide electrode placement in NCS, such as in the case of lateral cutaneous nerve of the thigh, which may otherwise difficult to obtain (Fig. 14) (Park et al., 2015).

7. Conclusion

The safety, ease of accessibility, and dynamic nature of ultrasound has led to its increasing use, and knowledge of this growing field will soon become a necessity in the practice of neuromuscular medicine. Ultrasonography is a painless, point of care extension of the physical and electrodiagnostic examinations that provides structural information. Although it is most commonly used in the diagnosis of focal neuropathies, the field of NMUS has expanded to include polyneuropathy, myopathy, and motor neuron disease. Although the quality of ultrasound study is dependent on operator experience, the development of quantitative measures appears promising in its ability to improve patient care.

Declaration of Competing Interest

None.

Acknowledgments

The authors thank Paul Zwelling for his contribution to ultrasound images.

Author agreement

Both authors participated in a meaningful way (both performed literature review, obtained ultrasound images, and contributed to the manuscript). The article is the authors' original work, has not received prior publication and is not under consideration for publication elsewhere. All authors have approved the final article.

References

Alrajeh, M., Preston, D.C., 2018. Neuromuscular ultrasound in electrically non-localizable ulnar neuropathy. Muscle Nerve 58, 655–659. https://doi.org/10.1002/mus.26291.

Alter, K.E., Karp, B., Hallett, M., Lungu, C., 2013. Ultrasound-Guided Chemodenervation Procedures: Text and Atlas. Demos Medical Publishing, New York, NY.

Arts, I.M.P., Overeem, S., Pillen, S., Jurgen Schelhaas, H., Zwarts, M.J., 2011. Muscle changes in amyotrophic lateral sclerosis: a longitudinal ultrasonography study. Clin. Neurophysiol. 122, 623–628. https://doi.org/10.1016/j.clinph.2010.07.023.

Arts, I.M.P., Overeem, S., Pillen, S., Kleine, B.U., Boekestein, W.A., Zwarts, M.J., Jurgen Schelhaas, H., 2012. Muscle ultrasonography: a diagnostic tool for amyotrophic lateral sclerosis. Clin. Neurophysiol. 123, 1662–1667. https://doi.org/10.1016/j.clinph.2011.11.262.

Bartels, R.H.M.A., Meulstee, J., Verhagen, W.I.M., Luttikhuis, T.T.M.C.-O., 2008. Ultrasound imaging of the ulnar nerve: correlation of preoperative and intraoperative dimensions. Clin. Neurol. Neurosurg. 110, 687–690. https://doi.org/10.1016/j.clineuro.2008.04.003.

Baute, V., Strakowski, J.A., Reynolds, J.W., Karvelas, K.R., Ehlers, P., Brenzy, K.J., Li, Z.J., Cartwright, M.S., 2018. Neuromuscular ultrasound of the brachial plexus: A standardized approach. Muscle Nerve 58, 618–624. https://doi.org/10.1002/mus.26144.

Bayrak, I.K., Bayrak, A.O., Kale, M., Turker, H., Diren, B., 2008. Bifid median nerve in patients with carpal tunnel syndrome. J. Ultrasound Med. 27, 1129–1136. https://doi.org/10.7863/jum.2008.27.8.1129.

Beekman, R., Visser, L.H., Verhagen, W.I., 2011. Ultrasonography in ulnar neuropathy at the elbow: a critical review. Muscle Nerve 43, 627–635. https://doi.org/10.1002/mus.22019.

Bhansing, K.J., Van Rosmalen, M.H., Van Engelen, B.G., Vonk, M.C., Van Riel, P.L., Pillen, S., 2015. Increased fascial thickness of the deltoid muscle in dermatomyositis and polymyositis: An ultrasound study. Muscle Nerve 52, 534–539. https://doi.org/10.1002/mus.24595.

Billakota, S., Hobson-Webb, L.D., 2017. Standard median nerve ultrasound in carpal tunnel syndrome: A retrospective review of 1021 cases. Clin. Neurophysiol. Pract. 2, 188–191. https://doi.org/10.1016/j.cnp.2017.07.004.

Bland, J.D.P., Rudolfer, S.M., 2014. Ultrasound imaging of the median nerve as a prognostic factor for carpal tunnel decompression. Muscle Nerve 49, 741–744. https://doi.org/10.1002/mus.24058.

Bönnemann, C.G., Brockmann, K., Hanefeld, F., 2003. Muscle ultrasound in Bethlem myopathy. Neuropediatrics 34, 335–336. https://doi.org/10.1055/s-2003-44665.

Boon, A.J., Harper, C.J., Ghahfarokhi, L.S., Strommen, J.A., Watson, J.C., Sorenson, E.J., 2013. Two-dimensional ultrasound imaging of the diaphragm: quantitative values in normal subjects. Muscle Nerve 47, 884–889. https://doi.org/10.1002/mus.23702.

Boon, A.J., O'Gorman, C., 2016. Ultrasound in the Assessment of Respiration. J. Clin. Neurophysiol. 33, 112–119. https://doi.org/10.1097/WNP.0000000000000240.

Boon, A.J., Sekiguchi, H., Harper, C.J., Strommen, J.A., Ghahfarokhi, L.S., Watson, J.C., Sorenson, E.J., 2014. Sensitivity and specificity of diagnostic ultrasound in the diagnosis of phrenic neuropathy. Neurology 83, 1264–1270. https://doi.org/10.1212/WNL.0000000000000841.

Brandsma, R., Verbeek, R.J., Maurits, N.M., van der Hoeven, J.H., Brouwer, O.F., den Dunnen, W.F.A., Burger, H., Sival, D.A., 2014. Visual screening of muscle ultrasound images in children. Ultrasound Med. Biol. 40, 2345–2351. https://doi.org/10.1016/j.ultrasmedbio.2014.03.027.

Breiner, A., Qrimli, M., Ebadi, H., Alabdali, M., Lovblom, L.E., Abraham, A., Albulahi, H., Perkins, B.A., Bril, V., 2017. Peripheral nerve high-resolution ultrasound in diabetes. Muscle Nerve 55, 171–178. https://doi.org/10.1002/mus.25223.

Cartwright, M.S., Passmore, L.V., Yoon, J.-S., Brown, M.E., Caress, J.B., Walker, F.O., 2008. Cross-sectional area reference values for nerve ultrasonography. Muscle Nerve 37, 566–571. https://doi.org/10.1002/mus.21009.

Cartwright, M.S., Walker, F.O., Griffin, L.P., Caress, J.B., 2011a. Peripheral nerve and muscle ultrasound in amyotrophic lateral sclerosis. Muscle Nerve 44, 346–351. https://doi.org/10.1002/mus.22035.

Cartwright, M.S., White, D.L., Demar, S., Wiesler, E.R., Sarlikiotis, T., Chloros, G.D., Yoon, J.S., Won, S.J., Molnar, J.A., Defranzo, A.J., Walker, F.O., 2011b. Median nerve changes following steroid injection for carpal tunnel syndrome. Muscle Nerve 44, 25–29. https://doi.org/10.1002/mus.22067.

Chang, W.K., Li, Y.P., Zhang, D.F., Liang, B.S., 2017. The cubital tunnel syndrome caused by the intraneural or extraneural ganglion cysts: Case report and review of the literature. J. Plast. Reconstr. Aesthet. Surg. 70, 1404–1408. https://doi.org/10.1016/j.bjps.2017.05.006.

Dekelver, I., Van Glabbeek, F., Dijs, H., Stassijns, G., 2012. Bilateral ulnar nerve entrapment by the M. anconeus epitrochlearis. A case report and literature review. Clin. Rheumatol. 31, 1139–1142. https://doi.org/10.1007/s10067-012-1991-7.

Demondion, X., Herbinet, P., Boutry, N., Fontaine, C., Francke, J.-P., Cotten, A., 2003. Sonographic Mapping of the Normal Brachial Plexus. Am. J. Neuroradiol. 24, 1303–1309.

Dietz, A.R., Bucelli, R.C., Pestronk, A., Zaidman, C.M., 2016. Nerve ultrasound identifies abnormalities in the posterior interosseous nerve in patients with proximal radial neuropathies. Muscle Nerve 53, 379–383. https://doi.org/10.1002/mus.24778.

Dikici, A.S., Ustabasioglu, F.E., Delil, S., Nalbantoglu, M., Korkmaz, B., Bakan, S., Kula, O., Uzun, N., Mihmanli, I., Kantarci, F., 2017. Evaluation of the tibial nerve with shear-wave elastography: a potential sonographic method for the diagnosis of diabetic peripheral neuropathy. Radiology 282, 494–501. https://doi.org/10.1148/radiol.2016160135.

Elsaidi, G.A., Wiesler, E.R., 2004. Lipofibromatous hamartoma of the median nerve: case presentation of MRI, ultrasound, electrodiagnostic, histologic, and surgical findings. Am. J. Orthop. Belle Mead NJ 33, 514–516.

Fantino, O., 2014. Role of ultrasound in posteromedial tarsal tunnel syndrome: 81 cases. J. Ultrasound 17, 99–112. https://doi.org/10.1007/s40477-014-0082-9.

Filippou, G., Mondelli, M., Greco, G., Bertoldi, I., Frediani, B., Galeazzi, M., Giannini, F., 2010. Ulnar neuropathy at the elbow: how frequent is the idiopathic form? An ultrasonographic study in a cohort of patients. Clin. Exp. Rheumatol. 28, 63–67.

Fowler, J.R., Munsch, M., Tosti, R., Hagberg, W.C., Imbriglia, J.E., 2014. Comparison of ultrasound and electrodiagnostic testing for diagnosis of carpal tunnel syndrome: study using a validated clinical tool as the reference standard. J. Bone Jt. Surg. 96,. https://doi.org/10.2106/JBJS.M.01250 e148.

Frijlink, D.W., Brekelmans, G.J.F., Visser, L.H., 2013. Increased nerve vascularization detected by color Doppler sonography in patients with ulnar neuropathy at the elbow indicates axonal damage. Muscle Nerve 47, 188–193. https://doi.org/10.1002/mus.23505.

American Association of Neuromuscular & Electrodiagnostic Medicine [WWW Document], n.d. http://www.aanem.org/Practice/Glossary-of-Terms (accessed 3.10.19).

Goedee, H.S., Jongbloed, B.A., van Asseldonk, J.-T.H., Hendrikse, J., Vrancken, A.F.J.E., Franssen, H., Nikolakopoulos, S., Visser, L.H., van der Pol, W.L., van den Berg, L. H., 2017. A comparative study of brachial plexus sonography and magnetic resonance imaging in chronic inflammatory demyelinating neuropathy and multifocal motor neuropathy. Eur. J. Neurol. 24, 1307–1313. https://doi.org/10.1111/ene.13380.

González Pérez, I., Corella Montoya, F., Casado Fariñas, I., 2017. Intraneural microcystic lymphatic malformation of the ulnar nerve at the Guyon canal: Unusual cause of ulnar pain in a child. Orthop. Traumatol. Surg. Res. OTSR 103, 513–515. https://doi.org/10.1016/j.otsr.2017.01.016.

Granata, G., Pazzaglia, C., Calandro, P., Luigetti, M., Martinoli, C., Sabatelli, M., Padua, L., 2009. Ultrasound visualization of nerve morphological alteration at the site of conduction block. Muscle Nerve 40, 1068–1070. https://doi.org/10.1002/mus.21449.

Grant, T.H., Omar, I.M., Dumanian, G.A., Pomeranz, C.B., Lewis, V.A., 2015. Sonographic evaluation of common peroneal neuropathy in patients with foot drop. J. Ultrasound Med. 34, 705–711. https://doi.org/10.7863/ultra.34.4.705.

Grimm, A., Décard, B.F., Bischof, A., Axer, H., 2014. Ultrasound of the peripheral nerves in systemic vasculitic neuropathies. J. Neurol. Sci. 347, 44–49. https://doi.org/10.1016/j.jns.2014.09.017.

Grimm, A., Rattay, T.W., Winter, N., Axer, H., 2017. Peripheral nerve ultrasound scoring systems: benchmarking and comparative analysis. J. Neurol. 264, 243–253. https://doi.org/10.1007/s00415-016-8305-y.

Heckmatt, J.Z., Leeman, S., Dubowitz, V., 1982. Ultrasound imaging in the diagnosis of muscle disease. J. Pediatr. 101, 656–660. https://doi.org/10.1016/S0022-3476(82)80286-2.

Heckmatt, J.Z., Pier, N., Dubowitz, V., 1988. Real-time ultrasound imaging of muscles. Muscle Nerve 11, 56–65. https://doi.org/10.1002/mus.880110110.

Hobson-Webb, L.D., Juel, V.C., 2017. Common entrapment neuropathies. Continuum 23, 487–511. https://doi.org/10.1212/CON.0000000000000452.

Hobson-Webb, L.D., Massey, J.M., Juel, V.C., Sanders, D.B., 2008. The ultrasonographic wrist-to-forearm median nerve area ratio in carpal tunnel syndrome. Clin. Neurophysiol. 119, 1353–1357. https://doi.org/10.1016/j.clinph.2008.01.101.

Hobson-Webb, L.D., Walker, F.O., 2004. Traumatic neuroma diagnosed by ultrasonography. Arch. Neurol. 61, 1322–1323. https://doi.org/10.1001/archneur.61.8.1322.

Hwang, H.-E., Hsu, T.-R., Lee, Y.-H., Wang, H.-K., Chiou, H.-J., Niu, D.-M., 2017. Muscle ultrasound: A useful tool in newborn screening for infantile onset pompe disease. Medicine (Baltimore) 96,. https://doi.org/10.1097/MD.0000000000008415 e8415.

Jacobson, J., 2017. Fundamentals of Musculoskeletal Ultrasound. Elsevier, Philadelphia, PA.

Jansen, M., van Alfen, N., Nijhuis van der Sanden, M.W.G., van Dijk, J.P., Pillen, S., de Groot, I.J.M., 2012. Quantitative muscle ultrasound is a promising longitudinal follow-up tool in Duchenne muscular dystrophy. Neuromuscul. Disord. 22, 306–317. https://doi.org/10.1016/j.nmd.2011.10.020.

Johansson, M.T., Ellegaard, H.R., Tankisi, H., Fuglsang-Frederiksen, A., Qerama, E., 2017. Fasciculations in nerve and muscle disorders – A prospective study of muscle ultrasound compared to electromyography. Clin. Neurophysiol. 128, 2250–2257. https://doi.org/10.1016/j.clinph.2017.08.031.

Karvelas, K.R., Hommel, A.L., Cartwright, M.S., Walker, F.O., Hobson-Webb, L.D., 2018. Sonographic similarities of inclusion body myositis and myotonic dystrophy. Muscle Nerve 58, E25–E26. https://doi.org/10.1002/mus.26181.

Kele, H., Verheggen, R., Reimers, C.D., 2002. Carpal tunnel syndrome caused by thrombosis of the median artery: the importance of high-resolution ultrasonography for diagnosis. Case report. J. Neurosurg. 97, 471–473. https://doi.org/10.3171/jns.2002.97.2.0471.

Kerasnoudis, A., Pitarokoili, K., Behrendt, V., Gold, R., Yoon, M.-S., 2015a. Bochum ultrasound score versus clinical and electrophysiological parameters in distinguishing acute-onset chronic from acute inflammatory demyelinating polyneuropathy. Muscle Nerve 51, 846–852. https://doi.org/10.1002/mus.24484.

Kerasnoudis, A., Pitarokoili, K., Gold, R., Yoon, M.-S., 2015b. Nerve ultrasound and electrophysiology for therapy monitoring in chronic inflammatory demyelinating polyneuropathy. J. Neuroimaging 25, 931–939. https://doi.org/10.1111/jon.12279.

Lee, H., Brekelmans, G.J.F., Visser, L.H., 2016. Quantitative assessment of nerve echogenicity as an additional tool for evaluation of common fibular neuropathy. Clin. Neurophysiol. 127, 874–879. https://doi.org/10.1016/j.clinph.2015.03.019.

Leis, A.A., Smith, B.E., Kosiorek, H.E., Omejec, G., Podnar, S., 2017. Complete dislocation of the ulnar nerve at the elbow: a protective effect against neuropathy? Muscle Nerve 56, 242–246. https://doi.org/10.1002/mus.25483.

Liu, M.-T., Lee, J.-T., Wang, C.-H., Lin, Y.-C., Chou, C.-H., 2016. Cubital tunnel syndrome caused by ulnar nerve schwannoma in a patient with diabetic sensorimotor polyneuropathy. Acta Neurol. Taiwan 25, 60–64.

Lugão, H.B., Frade, M.A.C., Mazzer, N., Foss, N.T., Nogueira-Barbosa, M.H., 2017. Leprosy with ulnar nerve abscess: ultrasound findings in a child. Skeletal Radiol. 46, 137–140. https://doi.org/10.1007/s00256-016-2517-1.

Mallouhi, A., Pülzl, P., Pültzl, P., Trieb, T., Piza, H., Bodner, G., 2006. Predictors of carpal tunnel syndrome: accuracy of gray-scale and color Doppler sonography. Am. J. Roentgenol. 186, 1240–1245. https://doi.org/10.2214/AJR.04.1715.

Martínez-Payá, J.J., Del Baño-Aledo, M.E., Ríos-Díaz, J., Tembl-Ferrairó, J.I., Vázquez-Costa, J.F., Medina-Mirapeix, F., 2017. Muscular echovariation: a new biomarker in amyotrophic lateral sclerosis. Ultrasound Med. Biol. 43, 1153–1162. https://doi.org/10.1016/j.ultrasmedbio.2017.02.002.

Martinoli, C., Derchi, L.E., Bertolotto, M., Gandolfo, N., Bianchi, S., Fiallo, P., Nunzi, E., 2000. US and MR imaging of peripheral nerves in leprosy. Skeletal Radiol. 29, 142–150.

Meng, C., Adler, R., Peterson, M., Kagen, L., 2001. Combined use of power Doppler and gray-scale sonography: a new technique for the assessment of inflammatory myopathy. J. Rheumatol. 28, 1271–1282.

Mhoon, J.T., Juel, V.C., Hobson-Webb, L.D., 2012. Median nerve ultrasound as a screening tool in carpal tunnel syndrome: correlation of cross-sectional area measures with electrodiagnostic abnormality. Muscle Nerve 46, 871–878. https://doi.org/10.1002/mus.23426.

Misawa, S., Noto, Y., Shibuya, K., Isose, S., Sekiguchi, Y., Nasu, S., Kuwabara, S., 2011. Ultrasonographic detection of fasciculations markedly increases diagnostic sensitivity of ALS. Neurology 77, 1532–1537. https://doi.org/10.1212/WNL.0b013e318233b36a.

Mittal, G.A., Wadhwani, R., Shroff, M., Sukthankar, R., Pathan, E., Joshi, V.R., 2003. Ultrasonography in the diagnosis and follow-up of idiopathic inflammatory myopathies–a preliminary study. J. Assoc. Phys. India 51, 252–256.

Nakamichi, K., Tachibana, S., 1995. Restricted motion of the median nerve in carpal tunnel syndrome. J. Hand Surg. 20, 460–464. https://doi.org/10.1016/S0266-7681(05)80153-6.

Nodera, H., Takamatsu, N., Shimatani, Y., Mori, A., Sato, K., Oda, M., Terasawa, Y., Izumi, Y., Kaji, R., 2014. Thinning of cervical nerve roots and peripheral nerves in ALS as measured by sonography. Clin. Neurophysiol. 125, 1906–1911. https://doi.org/10.1016/j.clinph.2014.01.033.

Noto, Y.-I., Shiga, K., Tsuji, Y., Kondo, M., Tokuda, T., Mizuno, T., Nakagawa, M., 2014. Contrasting echogenicity in flexor digitorum profundus-flexor carpi ulnaris: a diagnostic ultrasound pattern in sporadic inclusion body myositis. Muscle Nerve 49, 745–748. https://doi.org/10.1002/mus.24056.

O'brien, T.G., Cazares Gonzalez, M.L., Ghosh, P.S., Mandrekar, J., Boon, A.J., 2017. Reliability of a novel ultrasound system for gray-scale analysis of muscle. Muscle Nerve 56, 408–412. https://doi.org/10.1002/mus.25513.

O'Gorman, C.M., O'brien, T.G., Boon, A.J., 2017. Utility of diaphragm ultrasound in myopathy. Muscle Nerve 55, 427–429. https://doi.org/10.1002/mus.25429.

O'gorman, C.M., Weikamp, J.G., Baria, M., Van Den Engel-Hoek, L., Kassardjian, C., Van Alfen, N., Boon, A.J., 2017. Detecting fasciculations in cranial nerve innervated muscles with ultrasound in amyotrophic lateral sclerosis. Muscle Nerve 56, 1072–1076. https://doi.org/10.1002/mus.25676.

Omejec, G., Podnar, S., 2016. What causes ulnar neuropathy at the elbow? Clin. Neurophysiol. 127, 919–924. https://doi.org/10.1016/j.clinph.2015.05.027.

Omejec, G., Podnar, S., 2015. Precise localization of ulnar neuropathy at the elbow. Clin. Neurophysiol. 126, 2390–2396. https://doi.org/10.1016/j.clinph.2015.01.023.

Padua, L., Di Pasquale, A., Liotta, G., Granata, G., Pazzaglia, C., Erra, C., Briani, C., Coraci, D., De Franco, P., Antonini, G., Martinoli, C., 2013. Ultrasound as a useful tool in the diagnosis and management of traumatic nerve lesions. Clin. Neurophysiol. 124, 1237–1243. https://doi.org/10.1016/j.clinph.2012.10.024.

Padua, L., Liotta, G., Di Pasquale, A., Granata, G., Pazzaglia, C., Caliandro, P., Martinoli, C., 2012. Contribution of ultrasound in the assessment of nerve diseases. Eur. J. Neurol. 19, 47–54. https://doi.org/10.1111/j.1468-1331.2011.03421.x.

Park, B.J., Joeng, E.S., Choi, J.K., Kang, S., Yoon, J.S., Yang, S.N., 2015. Ultrasound-guided lateral femoral cutaneous nerve conduction study. Ann. Rehabil. Med. 39, 47–51. https://doi.org/10.5535/arm.2015.39.1.47.

Pelosi, L., Tse, D.M.Y., Mulroy, E., Chancellor, A.M., Boland, M.R., 2018. Ulnar neuropathy with abnormal non-localizing electrophysiology: Clinical, electrophysiological and ultrasound findings. Clin. Neurophysiol. 129, 2155–2161. https://doi.org/10.1016/j.clinph.2018.07.020.

Pigula-Tresansky, A.J., Wu, J.S., Kapur, K., Darras, B.T., Rutkove, S.B., Anthony, B.W., 2018. Muscle compression improves reliability of ultrasound echo intensity. Muscle Nerve 57, 423–429. https://doi.org/10.1002/mus.25779.

Pillen, S., Arts, I.M.P., Zwarts, M.J., 2008. Muscle ultrasound in neuromuscular disorders. Muscle Nerve 37, 679–693. https://doi.org/10.1002/mus.21015.

Pillen, S., Morava, E., Van Keimpema, M., Ter Laak, H.J., De Vries, M.C., Rodenburg, R. J., Zwarts, M.J., 2006a. Skeletal muscle ultrasonography in children with a dysfunction in the oxidative phosphorylation system. Neuropediatrics 37, 142–147. https://doi.org/10.1055/s-2006-924512.

Pillen, S., van Dijk, J.P., Weijers, G., Raijmann, W., de Korte, C.L., Zwarts, M.J., 2009. Quantitative gray-scale analysis in skeletal muscle ultrasound: a comparison study of two ultrasound devices. Muscle Nerve 39, 781–786. https://doi.org/10.1002/mus.21285.

Pillen, Sigrid, van Keimpema, M., Nievelstein, R.A.J., Verrips, A., van Kruijsbergen-Raijmann, W., Zwarts, M.J., 2006b. Skeletal muscle ultrasonography: Visual versus quantitative evaluation. Ultrasound Med. Biol. 32, 1315–1321. https://doi.org/10.1016/j.ultrasmedbio.2006.05.028.

Pillen, S., Verrips, A., van Alfen, N., Arts, I.M.P., Sie, L.T.L., Zwarts, M.J., 2007. Quantitative skeletal muscle ultrasound: diagnostic value in childhood neuromuscular disease. Neuromuscul. Disord. 17, 509–516. https://doi.org/10.1016/j.nmd.2007.03.008.

Pinto, S., Alves, P., Pimentel, B., Swash, M., de Carvalho, M., 2016. Ultrasound for assessment of diaphragm in ALS. Clin. Neurophysiol. 127, 892–897. https://doi.org/10.1016/j.clinph.2015.03.024.

Poage, C., Roth, C., Scott, B., 2016. Peroneal Nerve Palsy: Evaluation and Management. J. Am. Acad. Orthop. Surg. 24, 1–10. https://doi.org/10.5435/JAAOS-D-14-00420.

Reimers, C.D., Fleckenstein, J.L., Witt, T.N., Müller-Felber, W., Pongratz, D.E., 1993. Muscular ultrasound in idiopathic inflammatory myopathies of adults. J. Neurol. Sci. 116, 82–92.

Ríos-Díaz, J., Del Baño-Aledo, M.E., Tembl-Ferrairó, J.I., Chumillas, M.J., Vázquez-Costa, J.F., Martínez-Payá, J.J., 2019. Quantitative neuromuscular ultrasound analysis as biomarkers in amyotrophic lateral sclerosis. Eur. Radiol. https://doi.org/10.1007/s00330-018-5943-8.

Samarawickrama, D., Therimadasamy, A.K., Chan, Y.C., Vijayan, J., Wilder-Smith, E. P., 2016. Nerve ultrasound in electrophysiologically verified tarsal tunnel syndrome. Muscle Nerve 53, 906–912. https://doi.org/10.1002/mus.24963.

Sanchez, J.E., Conkling, N., Labropoulos, N., 2011. Compression syndromes of the popliteal neurovascular bundle due to Baker cyst. J. Vasc. Surg. 54, 1821–1829. https://doi.org/10.1016/j.jvs.2011.07.079.

Scheidl, E., Böhm, J., Simó, M., Bereznai, B., Bereczki, D., Arányi, Z., 2014. Different patterns of nerve enlargement in polyneuropathy subtypes as detected by ultrasonography. Ultrasound Med. Biol. 40, 1138–1145. https://doi.org/10.1016/j.ultrasmedbio.2013.12.020.

Scheidl, E., Böhm, J., Simó, M., Rózsa, C., Bereznai, B., Kovács, T., Arányi, Z., 2012. Ultrasonography of MADSAM neuropathy: focal nerve enlargements at sites of existing and resolved conduction blocks. Neuromuscul. Disord. 22, 627–631. https://doi.org/10.1016/j.nmd.2012.03.005.

Scholten, R.R., Pillen, S., Verrips, A., Zwarts, M.J., 2003. Quantitative ultrasonography of skeletal muscles in children: normal values. Muscle Nerve 27, 693–698. https://doi.org/10.1002/mus.10384.

Schreiber, S., Abdulla, S., Debska-Vielhaber, G., Machts, J., Dannhardt-Stieger, V., Feistner, H., Oldag, A., Goertler, M., Petri, S., Kollewe, K., Kropf, S., Schreiber, F., Heinze, H.-J., Dengler, R., Nestor, P.J., Vielhaber, S., 2015. Peripheral nerve ultrasound in amyotrophic lateral sclerosis phenotypes. Muscle Nerve 51, 669–675. https://doi.org/10.1002/mus.24431.

Schreiber, S., Oldag, A., Kornblum, C., Kollewe, K., Kropf, S., Schoenfeld, A., Feistner, H., Jakubiczka, S., Kunz, W.S., Scherlach, C., Tempelmann, C., Mawrin, C., Dengler, R., Schreiber, F., Goertler, M., Vielhaber, S., 2013. Sonography of the median nerve in CMT1A, CMT2A, CMTX, and HNPP. Muscle Nerve 47, 385–395. https://doi.org/10.1002/mus.23681.

Simon, N.G., 2018. Treatment of ulnar neuropathy at the elbow - An ongoing conundrum. Clin. Neurophysiol. 129, 1716–1717. https://doi.org/10.1016/j.clinph.2018.06.006.

Sivak, W.N., Hagerty, S.E., Huyhn, L., Jordan, A.C., Munin, M.C., Spiess, A.M., 2016. Diagnosis of ulnar nerve entrapment at the arcade of struthers with electromyography and ultrasound. Plast. Reconstr. Surg. Glob. Open 4,. https://doi.org/10.1097/GOX.0000000000000628 e648.

Smidt, M.H., Visser, L.H., 2008. Carpal tunnel syndrome: clinical and sonographic follow-up after surgery. Muscle Nerve 38, 987–991. https://doi.org/10.1002/mus.20982.

Smith, E.C., Xixis, K.I., Grant, G.A., Grant, S.A., 2016. Assessment of obstetric brachial plexus injury with preoperative ultrasound. Muscle Nerve 53, 946–950. https://doi.org/10.1002/mus.24975.

Soni, N.J., Franco-Sadud, R., Schnobrich, D., Dancel, R., Tierney, D.M., Salame, G., Restrepo, M.I., McHardy, P., 2016. Ultrasound guidance for lumbar puncture. Neurol. Clin. Pract. 6, 358–368. https://doi.org/10.1212/CPJ.0000000000000265.

Sousa Neves, J., Santos Faria, D., Cerqueira, M., Afonso, M.C., Teixeira, F., 2018. Relevance of ultrasonography in assessing disease activity in patients with idiopathic inflammatory myopathies. Int. J. Rheum. Dis. 21, 233–239. https://doi.org/10.1111/1756-185X.13150.

Stewart, J.D., 1987. The variable clinical manifestations of ulnar neuropathies at the elbow. J. Neurol. Neurosurg. Psychiatry 50, 252–258.

Tagliafico, A., Altafini, L., Garello, I., Marchetti, A., Gennaro, S., Martinoli, C., 2010. Traumatic neuropathies: spectrum of imaging findings and postoperative assessment. Semin. Musculoskelet. Radiol. 14, 512–522. https://doi.org/10.1055/s-0030-1268071.

Tai, T.-W., Wu, C.-Y., Su, F.-C., Chern, T.-C., Jou, I.-M., 2012. Ultrasonography for diagnosing carpal tunnel syndrome: a meta-analysis of diagnostic test accuracy. Ultrasound Med. Biol. 38, 1121–1128. https://doi.org/10.1016/j.ultrasmedbio.2012.02.026.

Tawfik, E.A., El Zohiery, A.K., Abouelela, A.A.K., 2016. Proposed sonographic criteria for the diagnosis of idiopathic tarsal tunnel syndrome. Arch. Phys. Med. Rehabil. 97, 1093–1099. https://doi.org/10.1016/j.apmr.2015.11.012.

Telleman, J.A., Grimm, A., Goedee, S., Visser, L.H., Zaidman, C.M., 2018. Nerve ultrasound in polyneuropathies. Muscle Nerve 57, 716–728. https://doi.org/10.1002/mus.26029.

Tsuji, Y., Noto, Y.-I., Shiga, K., Teramukai, S., Nakagawa, M., Mizuno, T., 2017. A muscle ultrasound score in the diagnosis of amyotrophic lateral sclerosis. Clin. Neurophysiol. 128, 1069–1074. https://doi.org/10.1016/j.clinph.2017.02.015.

van Alfen, N., Nienhuis, M., Zwarts, M.J., Pillen, S., 2011. Detection of fibrillations using muscle ultrasound: diagnostic accuracy and identification of pitfalls. Muscle Nerve 43, 178–182. https://doi.org/10.1002/mus.21863.

Van Den Engel-Hoek, L., Van Alfen, N., De Swart, B.J.M., De Groot, I.J.M., Pillen, S., 2012. Quantitative ultrasound of the tongue and submental muscles in children and young adults. Muscle Nerve 46, 31–37. https://doi.org/10.1002/mus.23277.

Vanderpool, D.W., Chalmers, J., Lamb, D.W., Whiston, T.B., 1968. Peripheral compression lesions of the ulnar nerve. J. Bone Joint Surg. Br. 50, 792–803.

Vill, K., Schessl, J., Teusch, V., Schroeder, S., Blaschek, A., Schoser, B., Müller-Felber, W., 2015. Muscle ultrasound in classic infantile and adult Pompe disease: a useful screening tool in adults but not in infants. Neuromuscul. Disord. 25, 120–126. https://doi.org/10.1016/j.nmd.2014.09.016.

Visser, L.H., 2006. High-resolution sonography of the common peroneal nerve: detection of intraneural ganglia. Neurology 67, 1473–1475. https://doi.org/10.1212/01.wnl.0000240070.98910.bc.

Vögelin, E., Nüesch, E., Jüni, P., Reichenbach, S., Eser, P., Ziswiler, H.-R., 2010. Sonographic follow-up of patients with carpal tunnel syndrome undergoing surgical or nonsurgical treatment: prospective cohort study. J. Hand Surg. 35, 1401–1409. https://doi.org/10.1016/j.jhsa.2010.06.010.

Walker, F.O., Donofrio, P.D., Harpold, G.J., Ferrell, W.G., 1990. Sonographic imaging of muscle contraction and fasciculations: a correlation with electromyography. Muscle Nerve 13, 33–39. https://doi.org/10.1002/mus.880130108.

Weber, M.-A., Jappe, U., Essig, M., Krix, M., Ittrich, C., Huttner, H.B., Huttner, B.H., Meyding-Lamadé, U., Hartmann, M., Kauczor, H.-U., Delorme, S., 2006. Contrast-enhanced ultrasound in dermatomyositis- and polymyositis. J. Neurol. 253, 1625–1632. https://doi.org/10.1007/s00415-006-0318-5.

Williams, E.H., Rosson, G.D., Hagan, R.R., Hashemi, S.S., Dellon, A.L., 2012. Soleal sling syndrome (proximal tibial nerve compression): results of surgical decompression. Plast. Reconstr. Surg. 129, 454–462. https://doi.org/10.1097/PRS.0b013e31823aeb21.

Williams, E.H., Williams, C.G., Rosson, G.D., Dellon, L.A., 2009. Anatomic site for proximal tibial nerve compression: a cadaver study. Ann. Plast. Surg. 62, 322–325. https://doi.org/10.1097/SAP.0b013e31817e9d81.

Zaidman, C.M., Al-Lozi, M., Pestronk, A., 2009. Peripheral nerve size in normals and patients with polyneuropathy: an ultrasound study. Muscle Nerve 40, 960–966. https://doi.org/10.1002/mus.21431.

Zaidman, C.M., Harms, M.B., Pestronk, A., 2013a. Ultrasound of inherited vs. acquired demyelinating polyneuropathies. J. Neurol. 260, 3115–3121. https://doi.org/10.1007/s00415-013-7123-8.

Zaidman, C.M., Holland, M.R., Anderson, C.C., Pestronk, A., 2008. Calibrated quantitative ultrasound imaging of skeletal muscle using backscatter analysis. Muscle Nerve 38, 893–898. https://doi.org/10.1002/mus.21052.

Zaidman, C.M., Malkus, E.C., Connolly, A.M., 2015. Muscle ultrasound quantifies disease progression over time in infants and young boys with duchenne muscular dystrophy. Muscle Nerve 52, 334–338. https://doi.org/10.1002/mus.24609.

Zaidman, C.M., Malkus, E.C., Siener, C., Florence, J., Pestronk, A., Al-Lozi, M., 2011. Qualitative and quantitative skeletal muscle ultrasound in late-onset acid maltase deficiency. Muscle Nerve 44, 418–423. https://doi.org/10.1002/mus.22088.

Zaidman, C.M., Pestronk, A., 2014. Nerve size in chronic inflammatory demyelinating neuropathy varies with disease activity and therapy response over time: a retrospective ultrasound study. Muscle Nerve 50, 733–738. https://doi.org/10.1002/mus.24227.

Zaidman, C.M., Seelig, M.J., Baker, J.C., Mackinnon, S.E., Pestronk, A., 2013b. Detection of peripheral nerve pathology: comparison of ultrasound and MRI. Neurology 80, 1634–1640. https://doi.org/10.1212/WNL.0b013e3182904f3f.

Zaidman, C.M., van Alfen, N., 2016. Ultrasound in the Assessment of Myopathic Disorders. J. Clin. Neurophysiol. 33, 103–111. https://doi.org/10.1097/WNP.0000000000000245.

Zaidman, C.M., Wu, J.S., Kapur, K., Pasternak, A., Madabusi, L., Yim, S., Pacheck, A., Szelag, H., Harrington, T., Darras, B.T., Rutkove, S.B., 2017. Quantitative muscle

ultrasound detects disease progression in Duchenne muscular dystrophy. Ann. Neurol. 81, 633–640. https://doi.org/10.1002/ana.24904.
Zaidman, C.M., Wu, J.S., Wilder, S., Darras, B.T., Rutkove, S.B., 2014. Minimal training is required to reliably perform quantitative ultrasound of muscle. Muscle Nerve 50, 124–128. https://doi.org/10.1002/mus.24117.
Zanette, G., Fabrizi, G.M., Taioli, F., Lauriola, M.F., Badari, A., Ferrarini, M., Cavallaro, T., Tamburin, S., 2018. Nerve ultrasound findings differentiate Charcot-Marie-Tooth disease (CMT) 1A from other demyelinating CMTs. Clin. Neurophysiol. 129, 2259–2267. https://doi.org/10.1016/j.clinph.2018.08.016.